JOURNAL OF GEOPHYSICAL RESEARCH, VOL. 104, NO. B12, PAGES 29,365-29,385, DECEMBER 10, 1999

Bouvet Triple Junction in the South Atlantic: Geology and evolution

Marco Ligi, Enrico Bonatti,[1] Giovanni Bortoluzzi, Gabriela Carrara, and Paola Fabretti
Istituto di Geologia Marina, Consiglio Nazionale delle Richerche, Bologna, Italy

Dolores Gilod
Department of Geophysics, Moscow State University, Moscow

Alexander A. Peyve, Sergej Skolotnev, and Natalia Turko
Geological Institute, Russian Academy of Sciences, Moscow

Abstract. The South American, African, and Antarctic lithospheric plates meet in the Bouvet Triple Junction (BTJ) located in the South Atlantic near the island of Bouvet. Multibeam, magnetic, gravimetric, and seismic reflection data have been used to understand the evolution of the three accretionary/transform boundaries that converge in the BTJ. The easternmost segments of the American-Antarctic Ridge (AAR) have a spreading full rate of 19.5 mm/yr for the last 8 m.y. They are oriented N-S, except for some NE-SW segments, probably created by magma-poor extension. The southernmost portion of Mid-Atlantic Ridge (MAR) (spreading full rate of 30.5 mm/yr for the last 9 m.y.) has elevated topographic anomalies; it is segmented by transform and overlapping discontinuities and shows evidence of axial propagation. The MAR axial valley bifurcates at its southern tip in two branches oriented 115° and 180° that are, or have been up to recently, loci of crustal accretion. The bifurcation represents a former ridge-ridge-ridge (RRR) triple junction. The westernmost segments of the Southwest Indian Ridge (SWIR) are anomalously high. The segment adjacent to the island of Bouvet (spreading rate 14.5 mm/yr) is shallower than normal by almost 1 km due to the influence of the Bouvet hot spot. The westernmost SWIR segment (Spiess Ridge) consists of a "swollen" volcanic ridge that reaches 320 m below sea level and has a deep caldera on its summit. Spiess Ridge narrows and deepens to the NW; V-shaped topographic and magnetic lineations suggest that it propagates NW at a rate of 40 to 50 mm/yr. The Spiess magmatic event started at roughly 1 Ma, when it caused deactivation of the 115° spreading branch. Therefore the Antarctic, South American, and African plates meet presently not in a triple point but in a broad zone of diffuse deformation. An area of extensional deformation observed east of Spiess Ridge may be caused by excess crustal formation at Spiess Ridge that cannot be accommodated by motion of rigid plates. The evolution of the BTJ since 10 Ma involves stages of RRR, RFF and RRF configurations with highly variable geometry of the accretionary/transform boundaries. Topographic anomalies, anomalously thick crust and excess volcanism suggest that the upper mantle below this region is affected by widespread, strong thermal anomalies that have influenced the configuration of the BTJ, and determined indirectly intraplate deformation in wide areas of the BTJ region. The thermal anomaly that gave rise to the SWIR-Spiess excess magmatism is the prime cause of the recent disruption of a former RRR configuration, and of the imminent establishment of a new RRR Triple Junction to the north.

1. Introduction

The Antarctic plate is encircled by mostly accretionary plate boundaries; therefore, it is growing gradually. The processes by which it grows are particularly impressive in the few "triple junctions" (TJ) where the Antarctic plate meets two other major plates (Plate 1). This paper describes the geology of the Bouvet Triple Junction (BTJ), where the Antarctic, African, and South American lithospheric plates meet in a geologically complex region of the South Atlantic, located near Bouvet island. The southernmost segments of the Mid-Atlantic Ridge (MAR), with spreading halfrate of 16 mm/yr according to *Sclater et al.*[1976], meet in the BTJ with the westernmost segments of the SW Indian Ridge (SWIR), (spreading halfrate of 8 mm/yr) and with the easternmost branch of the American-Antarctic Ridge (AAR), with spreading halfrate of 9 mm/yr (Plate 1).

[1]Also at Lamont-Doherty Earth Observatory of Columbia University, Palisades, New York, and Department of Earth Sciences, University of Pisa, Pisa, Italy.

Paper number 1999JB900192.
0148-0227/99/1999JB900192$09.00

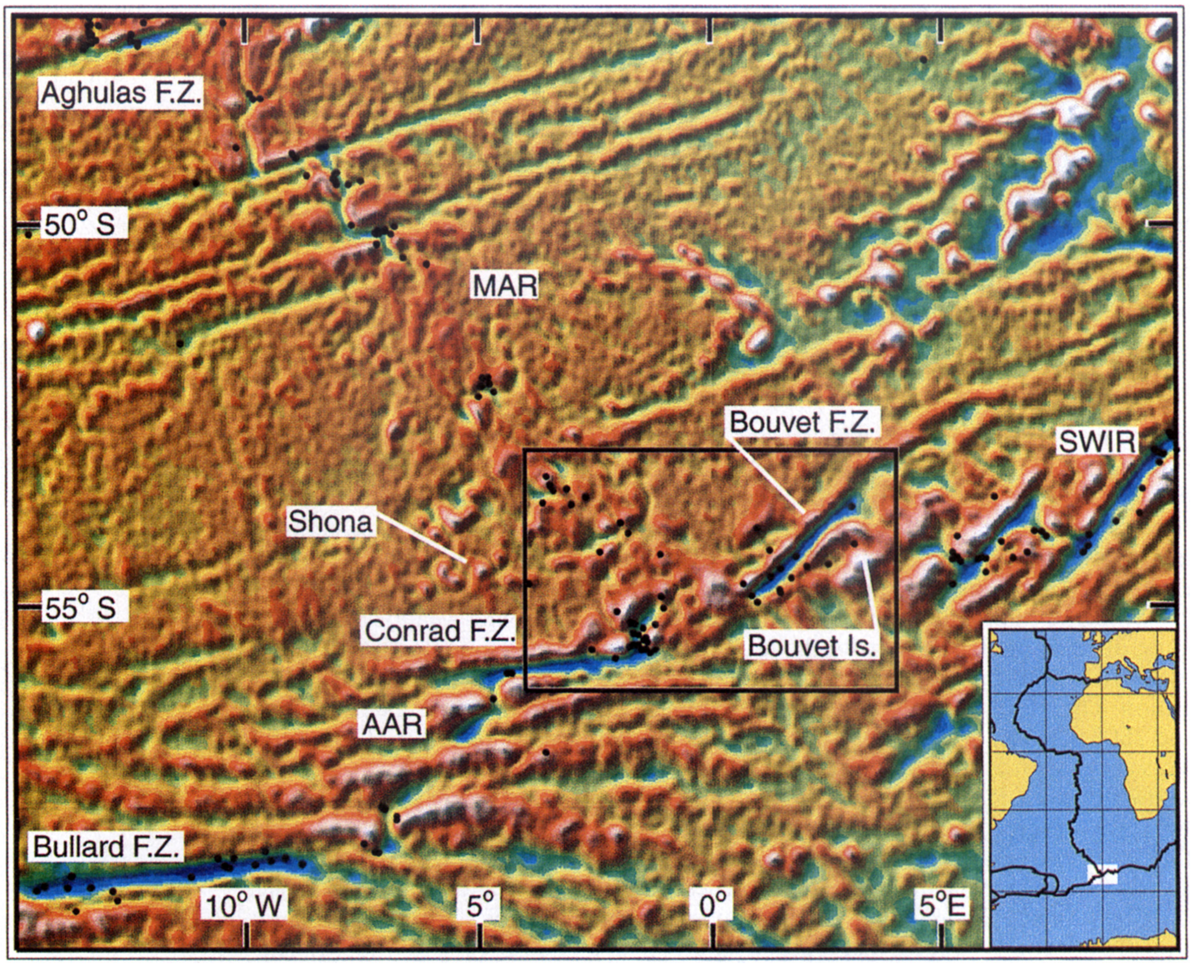

Plate1. Free-air gravity imagery derived from satellite altimetry data [*Sandwell and Smith*, 1997]. Dots are earthquake epicenters (magnitude >3) from the National Geophysical Data Center; they mark the boundaries between the African, South American and Antarctica plates. The survey area is shown in the inset.

The approximate location of the BTJ was estimated by *Johnson et al.*[1973] based on topography and magnetics and by *Forsyth* [1975] based on the distribution of earthquake epicenters. Its evolution in space and time has been studied by *Johnson et al.* [1973] and by *Sclater et al.* [1976]. They suggest that the present configuration of the BTJ is of ridge-transform-transform (RFF) type (terminology by *McKenzie and Morgan* [1969]) and that this configuration was prevalent during the last 20 m.y. except for some short lived shifts to a ridge-ridge-ridge (RRR) type. The main structural and petrological features of the AAR were discussed by *Lawver and Dick* [1983].

The geology of this region is further complicated by the inferred influence of one or more mantle plumes or hot spots. *Morgan* [1972] was the first to suggest that Bouvet island marks the present position of a mantle plume that has probably influenced the structure and composition of the westernmost SWIR and easternmost AAR [*Le Roex*, 1987; *Kurz et al.*, 1998]. The southernmost MAR may have been affected by hypothetical Shona and Discovery plumes, the latter being located at about 44°45'S, 6°45'W [*Le Roex*, 1987; *Douglass et al.*, 1995; *Small*, 1995]. Moreover, the evolution of the BTJ configuration may have been strongly influenced by the thermal/magmatic event that produced the SWIR-Spiess segment [*Ligi et al.*, 1997; *Mitchell and Livermore*, 1998a,b].

This paper presents results of two expeditions carried out to the Bouvet region under the sponsorship of the Italian Antarctic Research Program. The expeditions resulted from a collaboration between the Istituto di Geologia Marina of the Italian Research Council (CNR) and Moscow's Geology Institute of the Russian Academy of Sciences. The first took place in 1994 with the R/V *Akademik Strakhov* (cruise S18); the second took place in 1996 with the R/V *Gelendzhik* (cruise G96). Multibeam morphobathymetric, magnetic, gravimetric, and seismic reflection data, as well as bottom rock sampling, were obtained during these two expeditions.

2. Methods

Navigation was tracked with a Global Positioning System (GPS) Navstar satellite navigation system, with an accuracy of ±25 m. Morphobathymetry was obtained during the 1994

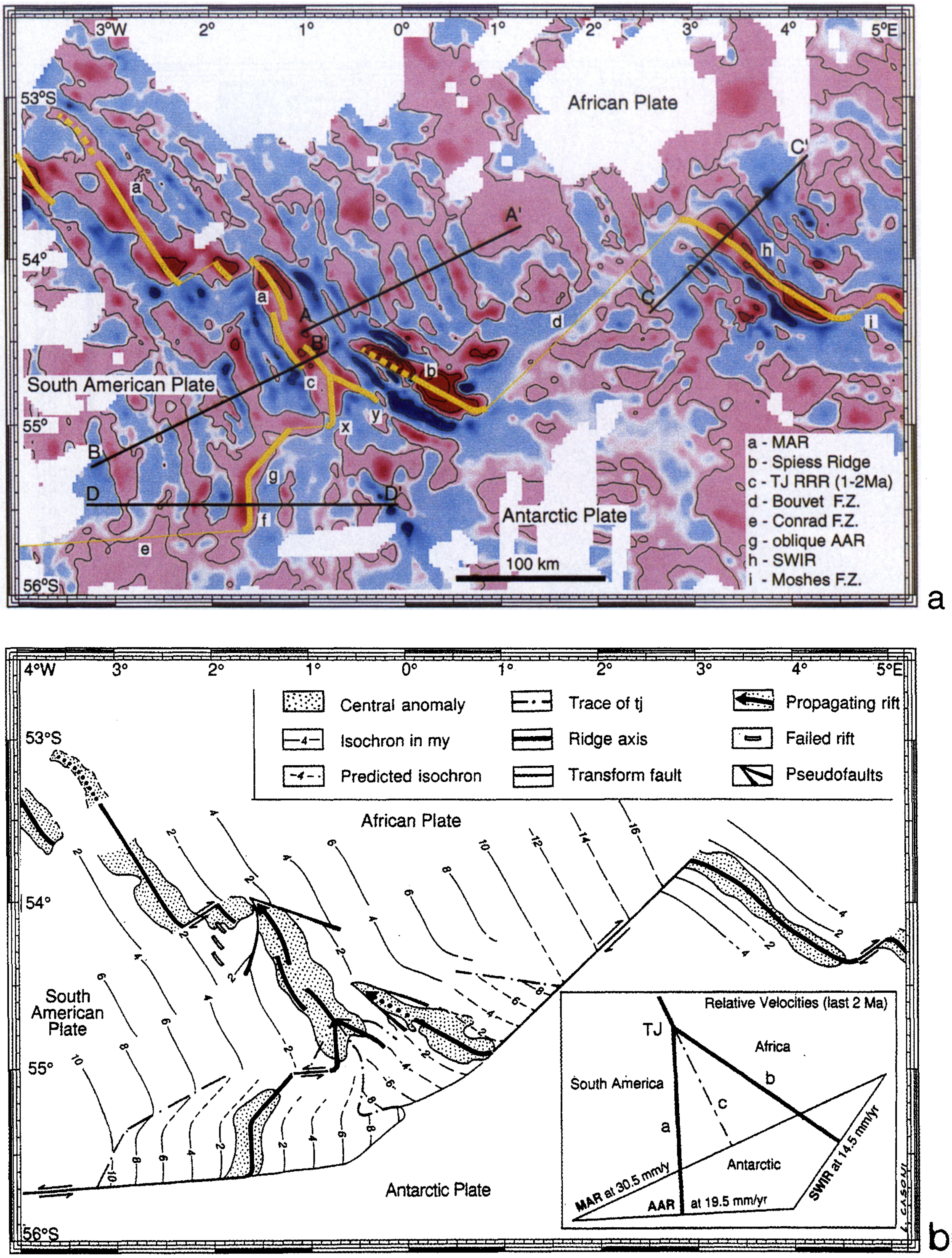

Plate 2. (a) Magnetic anomalies of Bouvet Triple Junction area (including *Sclater et al.*'s [1976] and our data). Red indicates positive magnetic anomalies, blue indicates negative anomalies, and contour interval is 500 nT. Yellow lines indicate the present-day plates boundaries (thick solid lines, ridge axis; thick dashed lines, assumed ridge axis; thin lines, transform faults). A-A', B-B', C-C', and D-D' indicate the location of magnetic profiles discussed in the text. The x and y are two small ridge segments at the southern tip of the MAR. (b) Tectonic boundaries and isochrons inferred from magnetic anomalies according to *Huestis and Acton*'s [1997] timescale. The present velocity triangle for the Bouvet Triple Junction and the relative geometry of the plate boundaries in a RRR configuration are shown in the inset. In this configuration, vectors **a** and **b** are the growth rates of the AAR and SWIR, respectively, and vector **c** is the rate that the MAR is consumed. The velocity triangle was obtained using the relative velocities computed from magnetic anomalies for the last 3 m.y. If we keep fixed the spreading direction of MAR (assumed to be normal to ridge axis) and of AAR (assumed parallel to Conrad FZ) and assuming plate rigidity, the closure of the velocity triangle requires a spreading direction for SWIR of 35°.

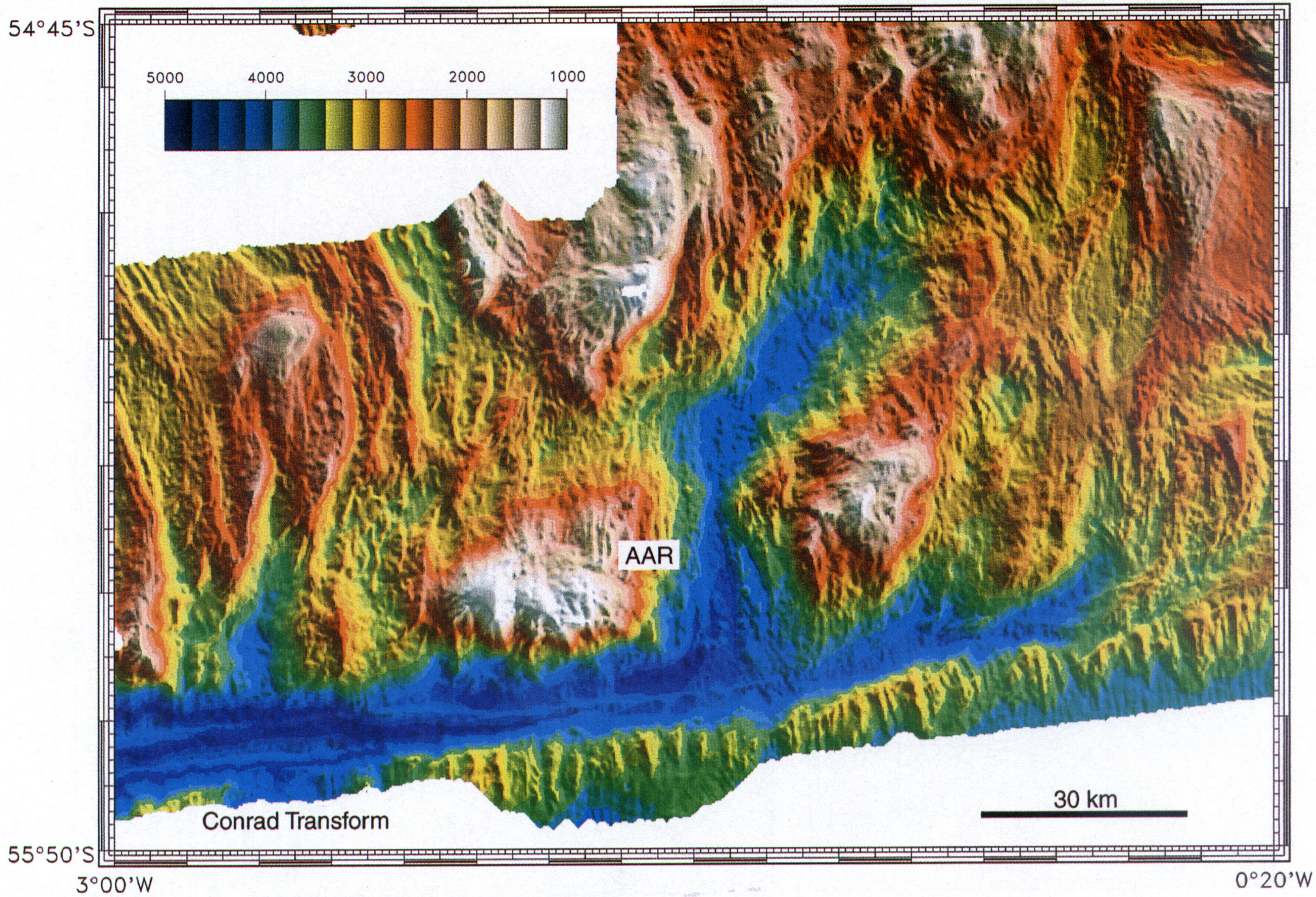

Plate 3. Shaded-relief image (source of light from NE) of the Conrad fracture zone and the AAR easternmost segment obtained from swath bathymetry data; grid resolution of 200 m. Color bar is in meters of depth below sea level. Note the AAR oblique spreading center.

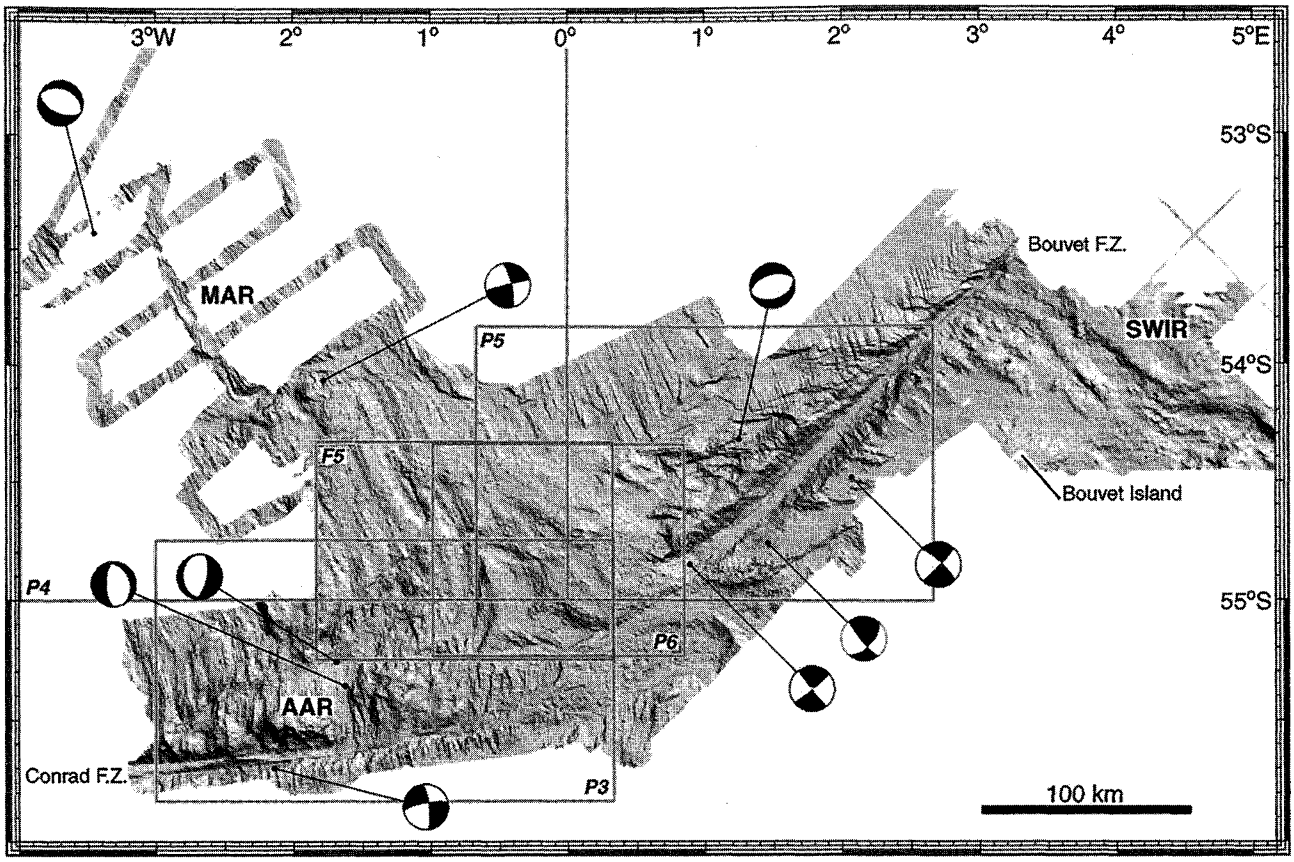

Figure 1. Shaded-relief image obtained using the swath bathymetry data of G96 and S18 cruises. Data are gridded at 200 m. Illumination from NE. Earthquake fault plane solutions from the Harvard Centroid Moment Tensor Catalog are indicated as focal mechanisms. Numbered boxes indicate different figures and plates in this paper, each with bathymetry of specific areas. The numbers indicate the figure/plate number.

cruise with a 15-beam Finnyard Echos 625 multibeam, covering a width of seafloor equal roughly to 2/3 the depth. During the 1996 cruise we employed a Simrad EM120S, 81-beam system, with a swath ~3-4 times the water depth. Processing of the multibeam data was carried out with the NEPTUNE-IRAP software of Simrad. The data underwent several cleaning and filtering steps before production of final grids and maps. In addition, we used the Generic Mapping Tools (GMT) [*Wessel and Smith*, 1991] and PLOTMAP [*Ligi and Bortoluzzi*, 1989] programs to produce other grids and maps.

Gravity was measured by a set of 4 Mod GMN-K gravimeters assembled by Vniigeofisika in Gelendzhik, Russia, mounted on gyroscopic platforms close to the ship's center of gravity, 0.7 m above sea level. The instruments were calibrated on known reference points with a portable Lacoste and Romberg G-327 gravimeter.

Two sets of magnetic data were recorded continuously by two towed magnetometers, one a Mod GSM-19MD of GEM, Ontario, the other a Proton Precession model MPM-7 built by NIPI Okeangeofisika.

Seismic reflection profiles were obtained in the 1994 cruise only, employing two Sodera GI guns as sound source. The receiving streamer employed 24 channels, each with 20 hydrophones, spaced 25 m apart. The seismic source was towed 6 m below the surface and 150 m from the nearest channel. Shot interval was 50 m, allowing sixfold coverage. Digital acquisition was carried out with a Geometrics 2420, with a sampling rate of 1 ms, a record length of 12 s, and an antialias filter of 180 Hz. This system operated at a speed of between 4 and 5 knots. In addition, single-channel seismic reflection data (50-m-long streamer) were acquired during multibeam surveys at speed of 10 knots. The seismic data were processed at the Istituto di Geologia Marina, CNR Bologna, using an industrial standard package (DISCO) made by Cogniseis. Rock sampling was carried out during both expeditions by conventional dredging, focused particularly along the accretionary and transform boundaries of the entire region.

3. Regional Morphostructural and Magnetometric Features

The Bouvet region includes the following structural areas (Plate 1): (1) easternmost segments of the AAR, (2) Southernmost segments of the MAR, (3) Westernmost segments of the SWIR, (4) Triple Junction area. A shaded relief image of the Bouvet region, based on our multibeam coverage, and a map of the magnetic anomalies based on our

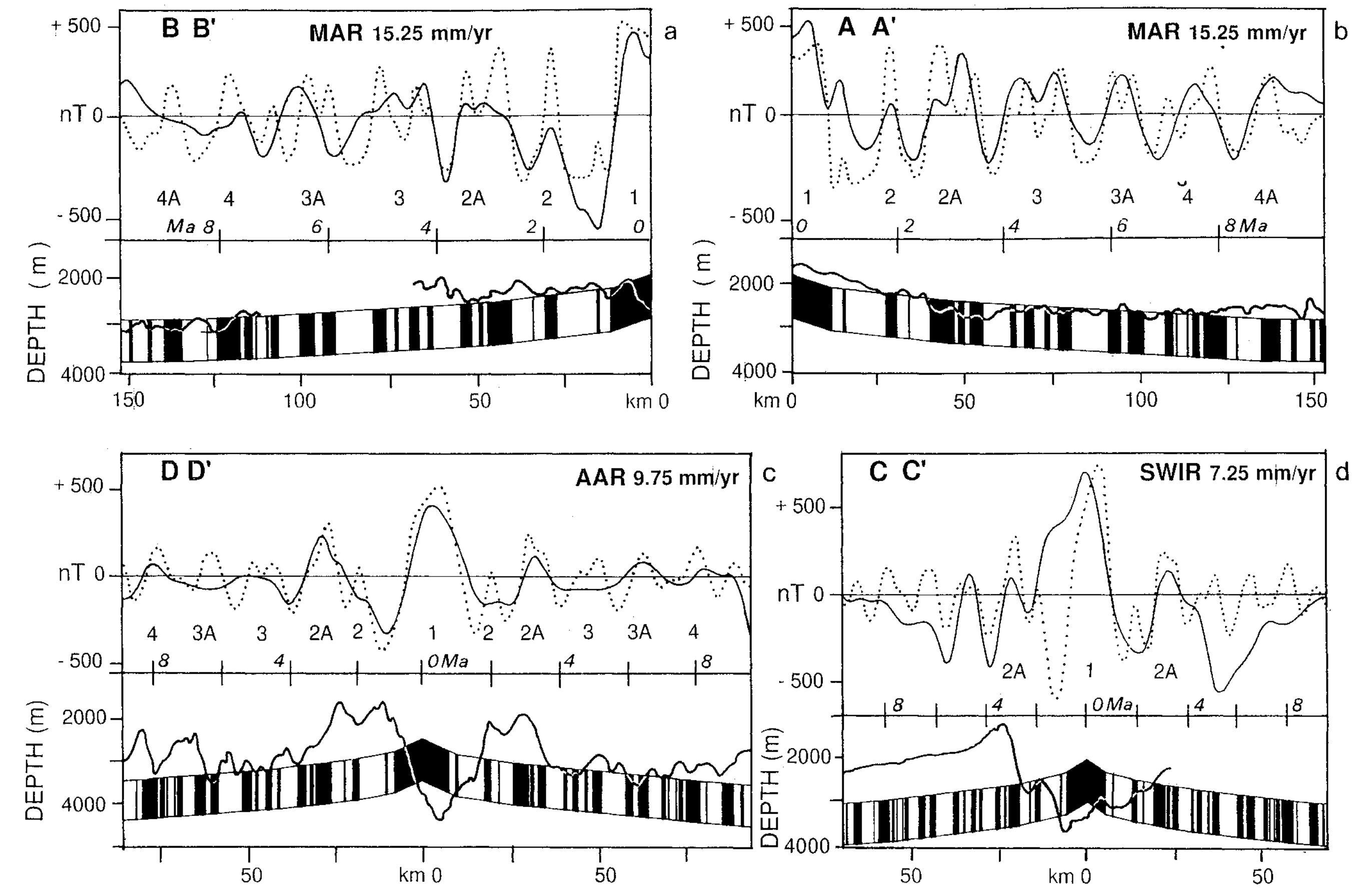

Figure 2. Profiles of topography/magnetic anomalies normal to (a) the MAR western sector (location of B-B' is indicated in Plate 2a), (b) the MAR eastern sector (A-A'), (c) the AAR north-south segment (D-D') and (d) the SWIR sector adjacent to Bouvet island (C-C'). Thick solid line, topography (vertical exaggeration 8 times); thin solid line, observed magnetic anomalies; dotted line, synthetic profile from the geological model superimposed on topography, based on *Huestis and Acton*'s [1997] timescale, assuming 1-km-thick magnetized layer and 15.25, 9.75 and 7.25 mm/yr half spreading rate for MAR, AAR, and SWIR, respectively.

data, complemented by data of *Sclater et al.* [1976] and *Johnson et al.* [1973], are shown in Figure 1 and Plate 2a. For the interpretation of the magnetic anomalies we followed the geomagnetic timescale of *Huestis and Acton* [1997]. A description of the four areas follows.

3.1. Easternmost American-Antarctic Ridge

The AAR [*Lawver and Dick*, 1983] is divided into several relatively short segments, trending about N-S, separated by transform offsets, one of which is the 200-km-long Conrad transform (Figure 1). A magnetic/topographic profile normal to the N-S AAR axial valley (profile D-D' in Plate 2a) gives an average full spreading rate of 19.5 mm/yr for the last 8 m.y. (Figure 2c). Satellite gravity imagery shows major oblique NE-SW depressions joining short N-S AAR segments (Plate 1); their significance is discussed briefly here, and more in depth by P.Fabretti et al. (manuscript in preparation, 1999).

3.1.1. Conrad transform. The Conrad transform strikes 87°. A U-shaped transform valley has a 10-km-wide floor, with two elongated troughs, >5500 m below sea level, separated by a transform-parallel median ridge (<4800 m below sea level). The northern trough shallows gradually moving eastward in the transform valley, and the valley narrows to ~5 km. The southern wall of the transform valley shows a saw-toothed pattern of alternating, elongated ridges and valleys oriented from 352° to 0°, i.e., roughly orthogonal to the transform valley. A major N-S valley enters the Conrad transform valley from the north roughly 75 km west of the eastern ridge/transform intersection (RTI). It might be an extinct ridge axis (Plate 3).

A prominent relief resembling an "inner corner high" is present at the eastern RTI: its flat top reaches 560 m below sea level (Plate 3). It is intensely tectonized, with two main systems of normal faults running roughly N-S and E-W. Its flat top may be related to erosion at sea level. Serpentinized peridotites, gabbros and basalts were recovered from the northern and southern slopes of this feature. The "outer corner low" of this RTI is, in fact, a topographic high, although less prominent than the inner corner high.

3.1.2. AAR oblique spreading segments. The easternmost AAR segment starting at the Conrad eastern RTI runs N-S for ~36 km; however, at about 55°20'S, its orientation changes sharply NE-SW for ~31 km (Plate 3). The N-S segment near the RTI has a 9-km-wide, 4500-m-deep axial valley that becomes shallower and narrower to the north.

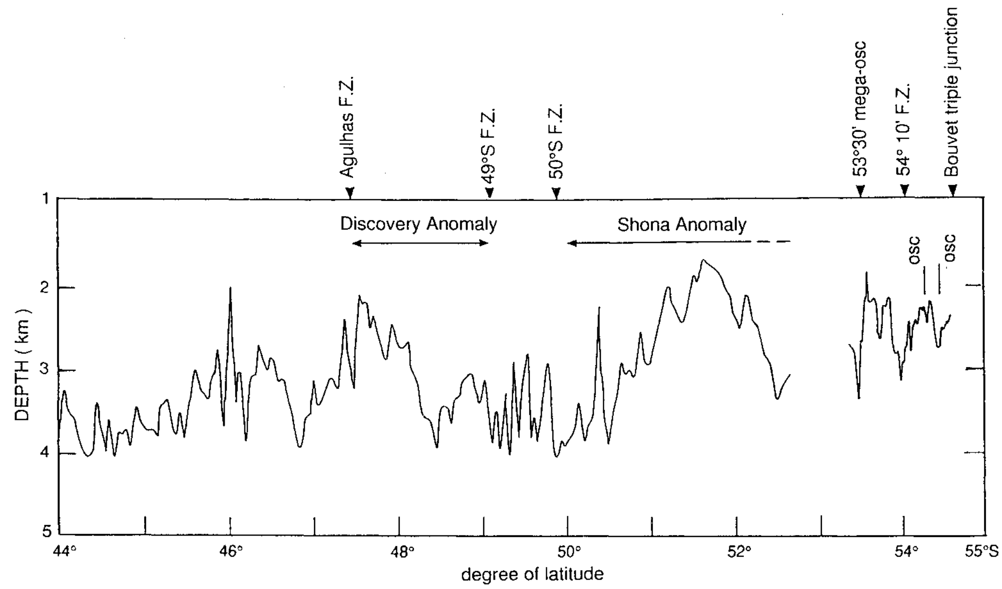

Figure 3. Zero-age axial topography of the MAR from 44°S to the triple junction area. Data north of 52°30'S are from *Douglass et al.* [1995]. Transform and overlapping spreading center (OSC) discontinuities are indicated.

The oblique segment is marked by a >4100 m deep valley oriented 37°. The valley floor displays two en echelon troughs oriented 15° to 17°. A positive magnetic anomaly and relatively high acoustic reflectivity suggest that this oblique trough is a locus of crustal emplacement. The oblique trough makes an angle of 48°-50° with the spreading direction (assumed to be parallel to the Bullard and Conrad transforms, and 90° from the direction of the linear magnetic anomalies). In the scheme of *Taylor et al.* [1994] it could be considered an oblique spreading center, rather than an extensional transform zone.

The oblique trough gives a strong signature in the satellite free-air gravity imagery (Plate 1), with a remarkable symmetry between the geometry of structures off the eastern and the western ends of the Conrad transform (i.e., in both cases a short N-S accretionary segment and NE-SW oblique trough). An oblique trough with the same NE-SW orientation is displayed by the AAR system south of 57°S in the satellite gravity imagery (Plate 1). It merges to the south with a short AAR segment north of the AAR-Bullard RTI. Thus three oblique, parallel structural segments are present between the Bullard transform and the BTJ area, marking probably an important regional structural direction of the AAR system that could be inherited from a complex interaction of lithospheric stresses and availability of magma within former triple junctions (P.Fabretti et al., manuscript in preparation, 1999).

3.2. Southernmost Mid-Atlantic Ridge

The segments of the MAR immediately north and south of the Agulhas-Falkland transform at 48°S are sharply outlined in the 7.2 version of *Sandwell and Smith*'s [1997] satellite free-air gravity imagery (Plate 1). However, the MAR signature loses its sharpness south of about 51°S, probably due to the absence of a well-formed deep axial rift valley.

3.2.1. MAR axis, propagation, and overlapping. The MAR north of about 53°S consists of relatively short ridge segments intersected by a number of small-offset (<50 km) transforms [*Douglass et al.*, 1995]. North of the Agulhas transform the MAR zero-age level ranges within "normal" values, i.e., between 3400 and 3800 m below sea level; however, between 47°S and 49°S, that is, south of the Agulhas transform, the ridge axis swells up to 2300-2500 m below sea level (Figure 3). A similar zero-age topographic anomaly was observed at 51°-52°S. These two topographic anomalies are associated with light-rare earth element (REE)-enriched mid-ocean ridge basalt (MORB) and have been ascribed to the influence of the Discovery and Shona mantle plumes, respectively [*Douglass et al.*, 1995].

Our multibeam and magnetic data indicate that the anomalously shallow MAR segments continue south of 53°S (Figure 3 and Plate 4). A NE-SW profile normal to the MAR at about 53°30'S reveals two prominent valleys, about 50 km apart, each associated with a positive magnetic anomaly. These en echelon twin depressions are visible in the satellite gravity imagery; two similar twin features can be observed on the axial zone of the MAR, also at about 52°30'S (Plate 1). In both cases the twin depressions are separated by a gravity high. It is possible that the two twin rift valleys are overlapping ridge segments, similar to those common on the East Pacific Rise [*Macdonald and Fox*, 1983], although the large distance between them (~50 km) would make this an unusual "megaoverlapping" system. Alternatively, they may be due to a recent ~50 km ridge jump. The southwestern twin segment has higher acoustic reflectivity and a stronger magnetic anomaly (Plate 2a). Moreover, very fresh basalt was recovered from it. Accordingly, this is probably the segment of MAR active at present. Immediately south, the MAR axis is displaced to the NE by about 40 km. A ~80-km-long segment follows (Plate 4), marked by a broad positive magnetic anomaly. Although no complete topographic coverage is available, it appears that this segment lacks a deep axial rift valley but has a broad, shallow depression with a central topographic high.

A small transform offsets the MAR by about 20 km at 54°10' S, producing a sort of nodal basin >4000 m below sea level. South of the 54°10'S transform the MAR axis consists of three "en echelon" segments separated by overlapping discontinuities (Plate 4). The central magnetic anomaly has secondary highs centered on each of the three segments. The distance between the overlappers is between 10 and 20 km. Magnetic/topographic profiles A-A' and B-B' (Plate 2a) give an average full spreading rate of 30.5 mm/yr for the last 9 m.y. (Figures 2a and 2b), a value close to that estimated by *Sclater et al.* 1976. On its NNW tip the northernmost overlapping segment, oriented 155°, shows features typical of a propagator, with two oblique, V-shaped topographic and magnetic lineations oriented 110° and 200°. They probably represent outer and inner pseudofaults [*Hey et al.*, 1980] that make a 45° angle with the propagating rift (inset in Plate 4), suggesting a rate of propagation similar to the half spreading rate, i.e., 15 mm/yr. Magnetic anomalies (rotated C2 at 54°20'S and 1°45'W) suggest that propagation started 2.5 m.y. before present (Plate 2). The outer pseudofault, marked by a sharp break in slope and by an offset of the magnetic anomalies, separates undeformed crust created by the propagating rift from crust created by the dying rift. The structural grain and the magnetic isochrons curve inward along the outer pseudofault, mimicking the inward (westward) curvature of the propagating tip (inset in Plate 4). The inner pseudofault is marked by a slightly depressed lineation that separates areas with different structural orientations.

The advancing segment is offset by ~30 km from the receding rift; the two overlap by <10 km creating a transform zone. The dying rift curves inward (eastward), in contrast to the kinematics model of *McKenzie* [1986]. The failed rift is made of a number of N-S, en echelon basins that together form a N-S depression; however, each basin curves inward (toward the propagating rift), suggesting episodic recession [*Wilson*, 1990].

The sheared zone between the propagating and the receding rifts is made of crust created by the receding rift, originally part of the African plate and transferred to the South American plate due to the northward migration of the transform zone. The sheared zone shows crustal blocks bound by faults oriented 150° in the northern part of the zone, curving gradually to 220° close to the failed rift. They may represent blocks that rotated due to "bookshelf tectonics", similar to those observed near the 95°30'W propagator in the Galapagos rift [*Kleinrock and Hey*, 1989].

A MAR-parallel morphostructural grain can be recognized NE of the axis (Figure 1) up to at least magnetic chron 4A (8.8 Ma). The southern tip of the MAR bifurcates in two short segments oriented about 115° and 180° (segments X and Y in Plate 2). Their significance is discussed in section 3.4.

3.2.2 Intraplate crustal deformation and extension east of the MAR. The ridge-parallel topography and magnetic stripes are disrupted in the SE flank of the southernmost MAR segment, due to the emplacement of the Spiess Ridge at the SW end of the Bouvet transform.

The morphostructural and magnetic lineations produced by the MAR do not reach the western portion of the Bouvet transform, being absent south of a roughly E-W line at 54°25'S (Figure 1). The lineations appear to have rotated parallel to the SWIR-Spiess segment within a triangle-shaped area limited by the 54°25'S E-W line to the north, by the Spiess Ridge to the west, and by a line running from the tip of the y ridge segment to the Spiess summit caldera and up to about 0°45'E (Plates 2 and 5). Eastward of this triangle-shaped area, a 60-km-wide strip of seafloor, parallel to the Bouvet transform, shows strong evidence of extensional tectonics (Plate 5). This extended zone is part of the African plate; therefore this tectonic deformation is intraplate.

The northern boundary of the extended zone consists of small grabens oriented SW-NE, which together form a depression parallel to the Bouvet transform. The northernmost graben connects with the Bouvet transform through a set of E-W low-angle normal faults dipping south. Moving toward the transform, these faults take a fan-like distribution; close to the transform they become normal to it.

Seismic profile BVT-13M (Figure 4) runs from the Antarctic plate across the Bouvet transform to the extended zone within the African plate (Plate 5b). The bottom of the sedimentary basin on the southern side of the Bouvet transform is made of blocks rotated on extensional faults (basin a in Figure 4). This extension is not active at present because the top of the sequence shows plane-parallel deposition on lap over the lower unconformity. The transform valley is filled by a 2-km-thick sediment pile, assuming an acoustic velocity of 2 km/s (basin b in Figure 4). Transcurrent motion is suggested by the different seismic facies and by a narrow zone of deformation of the sequence near the axis of the valley, similar to that detected in the sediments filling the Vema transform valley [*Eittreim and Ewing*, 1975]. Recent deposition in the transform valley appears to be affected by transcurrent tectonics only because recent reflectors are plane-parallel and in on-lap over the underlying sequence, and also because of the purely transcurrent motion shown by earthquake focal mechanisms (Figure 1). The seismic profile continues north of the Bouvet transform, i.e., in the extended zone, where it crosses one of the largest, presumably extensional basins. The basin is a half graben formed by the combined action of two master faults, one oriented E-W, the other WNW-ESE, with a total vertical slip of 1300 m (basin c in Figure 4). Depositional sequences are growing, and present-day strata are tilted and dip towards the fault surface, indicating recent extension, as suggested also by the focal mechanism for an earthquake located close to this basin (Figure 1). The seismic profile crosses also one of the grabens that form the northern depression within the extended zone (basin d in Figure 4). The principal faults of the graben cut the sedimentary sequence, suggesting recent extension. The fault with the largest vertical offset (in this profile about 700 m) is the northern boundary of the extended zone.

The predicted geometry of the magnetic anomalies is disrupted in the extended zone (Plate 2), possibly due to the intense deformation of this zone and circulation of fluids in the fractured crust. This notwithstanding, MAR accretionary structures are still recognizable, although they are affected by younger extensional faults. In conclusion, morphology, seismostratigraphy, and earthquakes distribution and focal mechanisms all suggest intense recent extensional brittle deformation, located not at the plate boundary (Bouvet transform) but distributed within the African plate throughout the extended zone.

3.3. Westernmost Southwest Indian Ridge

3.3.1. SWIR segment adjacent to Bouvet island. This 110-km-long segment runs from the Moshesh to the Bouvet transforms (Figure 1). Magnetic anomalies (profile C-C' in

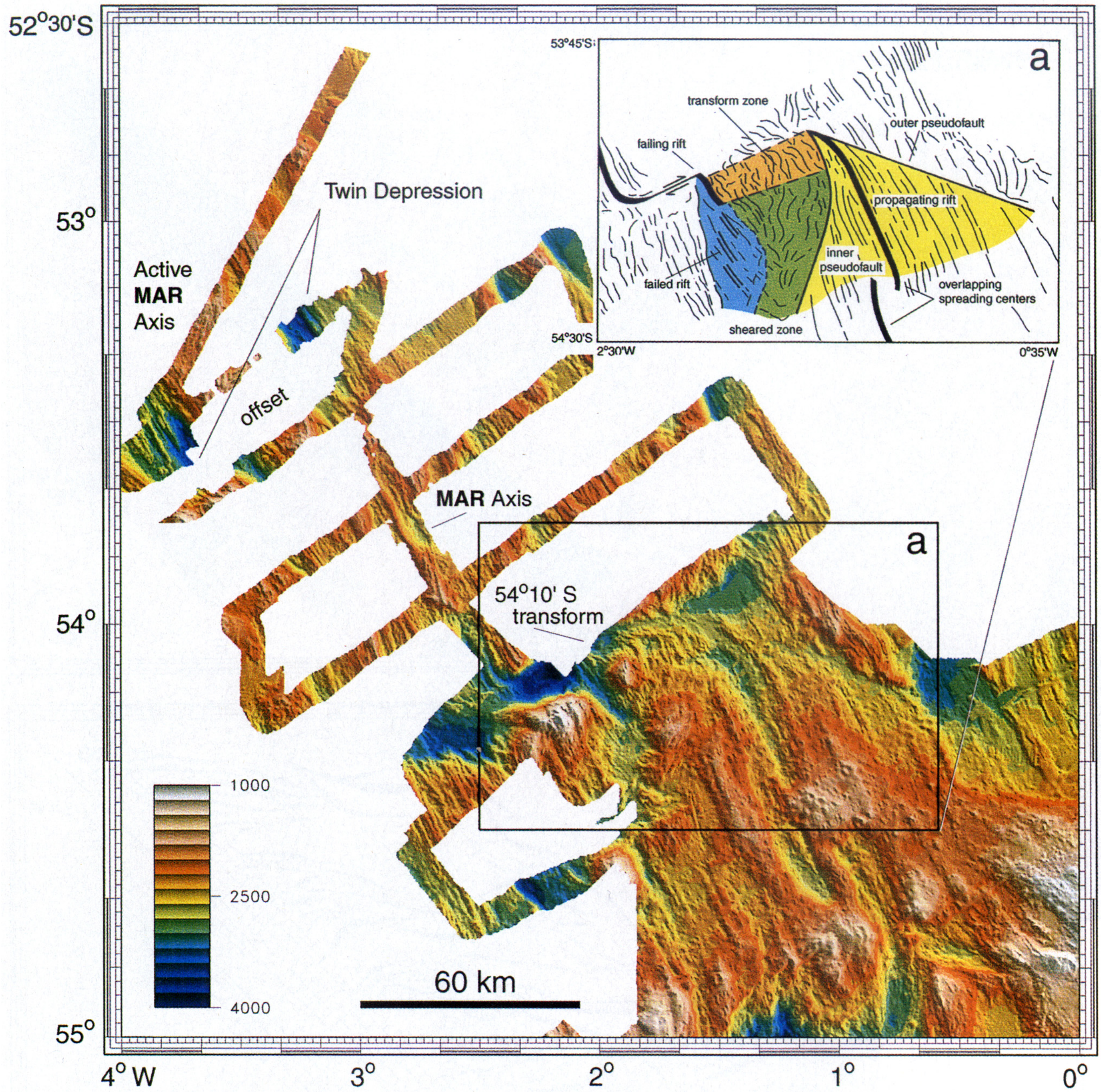

Plate 4. Shaded-relief image (source of light from NE) of the MAR segments from 52°30'S to the triple junction area obtained from swath bathymetry data; grid resolution of 200 m. Color bar is in meters of depth below sea level. Note the MAR axial discontinuities at different latitudes, the twin axial depression at 53°30'S, the northwestward propagation of MAR at 54°10'S, the overlapping spreading centers (from 54°10'S and 54°45'S); the axial MAR bifurcation south of 54°45'S. A line-drawing structural interpretation, with identified tectonic elements outlined by the box, is shown in the inset.

Plate 2a) give an average full spreading rate of 14.5 mm/yr for the last 3 m.y. (Figure 2d), close to the rate estimated by *Sclater et al.* [1976], with a slightly asymmetric spreading. The axial positive magnetic anomaly is narrow (~10 km) in the midpart of the segment and widens moving toward the transforms at the two edges of the segment (Plate 2a). This segment has a 1-km axial valley, typical of ridges with comparable low spreading rates. However, the valley is unusually broad (~16 km) and has a topographic high running along its axis (Figure 1). The axial magnetic anomaly is aligned along a linear depression running along the south-western side of this topographic high. Topography on the two sides of the ridge is asymmetric due to the presence on the SW side of the Bouvet island volcanic system.

The zero-age axis, identified by the axial magnetic anomaly, lies ~2000 m below sea level in the central part of

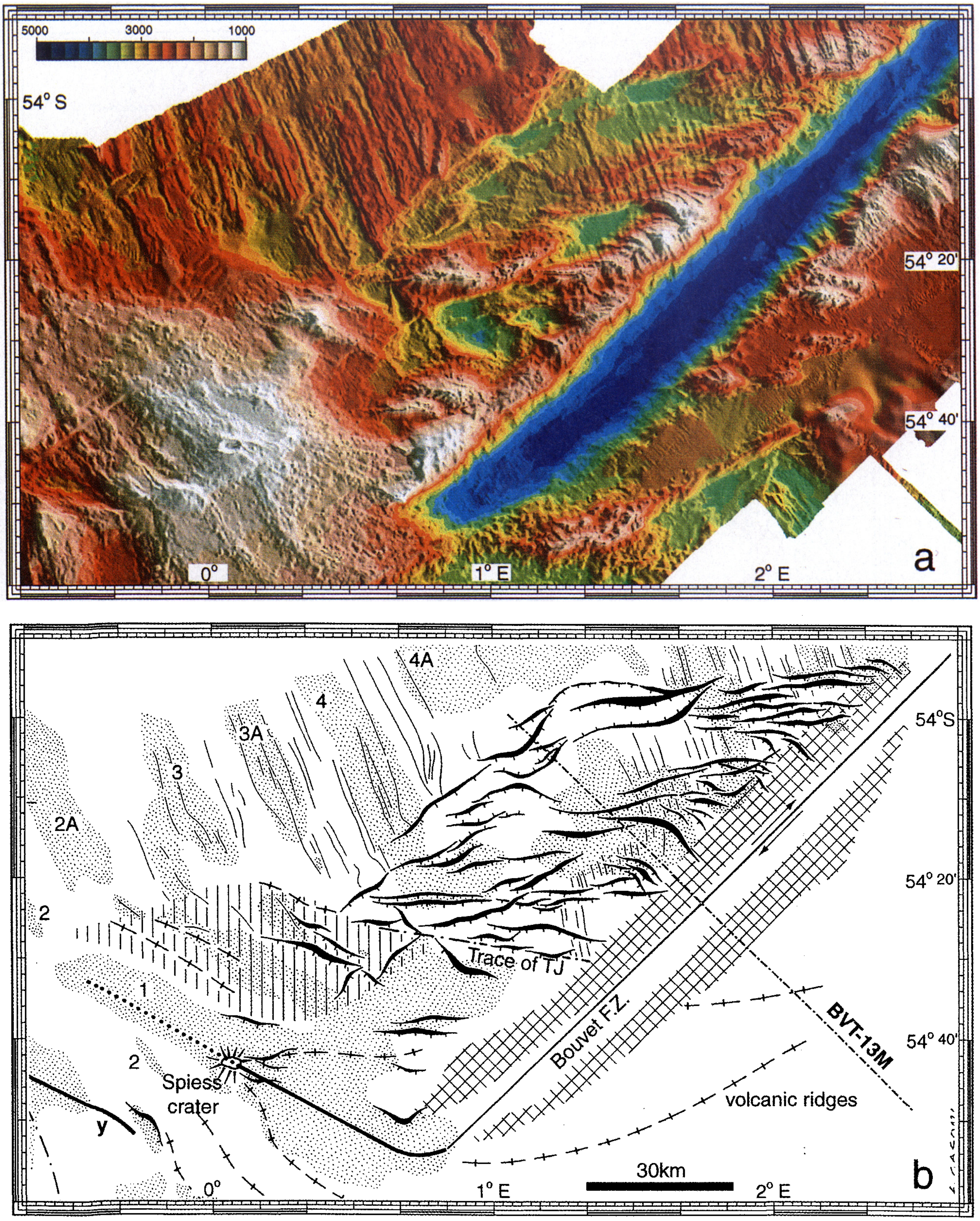

Plate 5. (a) Shaded-relief image (illumination from NE) of the Bouvet transform and SWIR segment east of Bouvet island, obtained from swath bathymetry data, grid resolution of 200 m. Color bar is in meters of depth below sea level. (b) Structural sketch map of the extended zone north of the Bouvet transform (African plate). The magnetic anomalies are indicated with dotted patterns, and magnetic chron indications are overprinted. Thin solid lines, MAR fabric; thick solid lines with hatches, normal faults; thick solid lines, ridge axis; thick dots, propagators; long dash-dotted line, trace of TJ; squared pattern, walls of the Bouvet transform valley; vertical solid line pattern, sheared zone; dash-dotted line, location of seismic reflection profile BVT-13M.

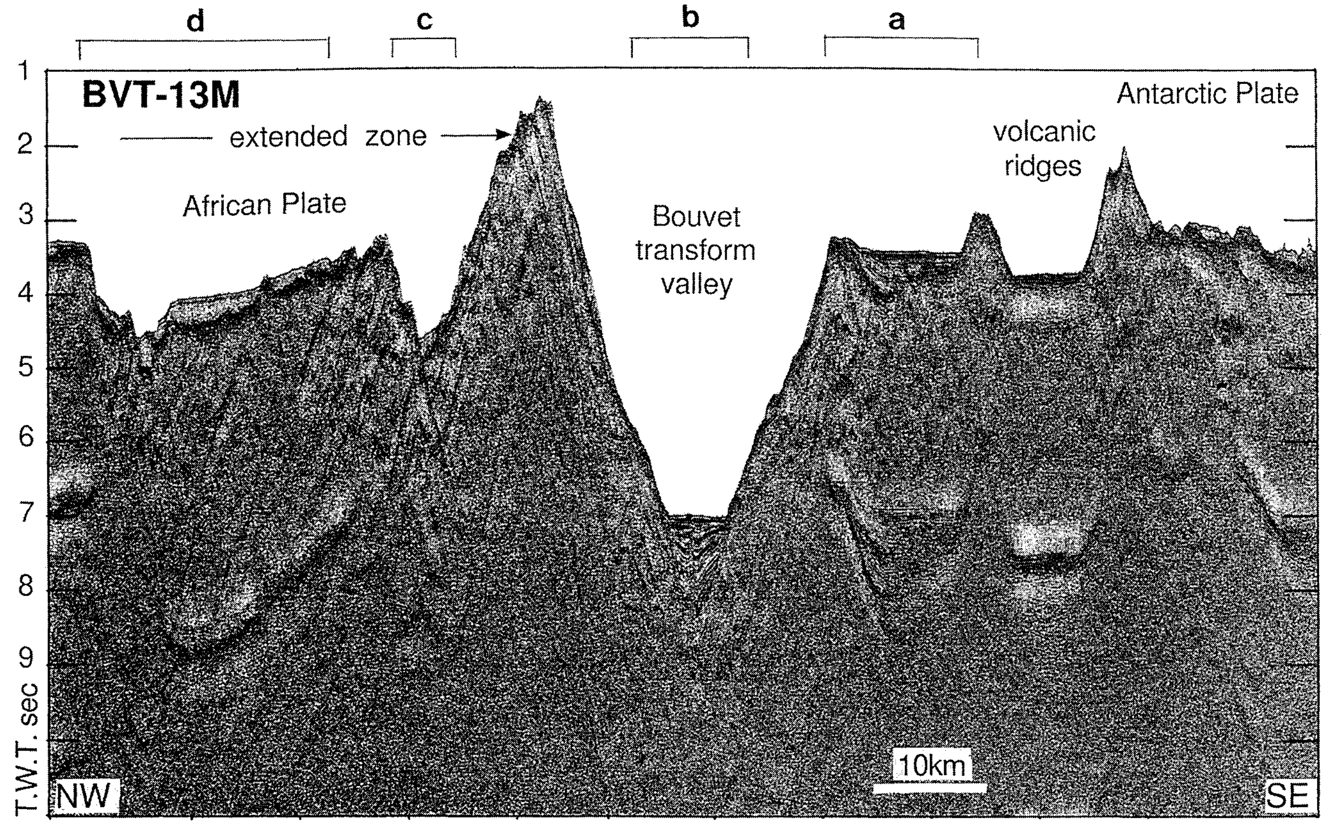

Figure 4. Multichannel seismic profile BVT-13M (finite difference time migrated section) across the Bouvet transform. Note the presence in the African plate of normal faults affecting both the basement and the sedimentary cover. See Plate 5b for location.

the segment and deepens slightly moving toward the intersections with the Bouvet and the Moshesh transforms (Figure 1). Thus this segment is shallower by about 1 km than mid ocean ridge segments with comparable spreading rates, probably due to a thick crust caused by anomalously high magma production related to the Bouvet melting anomaly.

3.3.2 Bouvet transform. This transform (offset length ~195 km) is the westernmost of a set of transforms oriented about N45°E offsetting the SWIR. The SWIR segment near Bouvet island deepens approaching the Bouvet transform, reaching 4600 m below sea level at the RTI. The bottom of the transform valley lies about 5400 m below sea level close to the midpart of the offset, where the valley contains a sediment pile up to 2000 m thick (Figure 4); thus the igneous basement below the valley lies over 7000 m below sea level. The valley disappears abruptly ~190 km SW of the NE RTI, probably dammed by young eruptives from the Spiess volcanic system. Sampling of the valley walls recovered serpentinized peridotites, gabbros, and basalts. Ultramafics had already been sampled from the southwestern side of the transform's wall by *Sclater et al.* [1978].

3.3.3. SWIR/Spiess Ridge. The segment of SWIR called Spiess Ridge is topographycally anomalous [*Sclater et al.*, 1976; *Mitchell et al.*, 1995; *Ligi et al.*, 1997; *Mitchell and Livermore*, 1998a, b]. Our multibeam survey indicates that Spiess Ridge is a complex volcanic system elongated toward NW, (i.e., parallel to the trend of the SWIR last few segments) and rising from ~2000 m to ~320 m below sea level (Plate 6). It is roughly 50 km wide at 2000 m below sea level, and it narrows and deepens toward NW. The summit shows a roughly elliptical 450 m deep crater or caldera about 4 per 3.5 km in diameter. Small eruptive cones can be identified on the flanks of the main edifice (Plate 6b). Fresh vesicular basalts, including strongly differentiated ferrobasalts, were recovered from this volcanic system by *Le Roex et al.* [1982] and by us.

A strong axial NW trending positive magnetic anomaly was detected over Spiess Ridge; it increases in intensity toward the NW tip of the ridge, off the central, more elevated part of the volcanic edifice (Plate 2a).The flanking negative anomalies show a V-shaped pattern suggesting propagation towards NW. The presence of ferrobasalts might contribute to the strong axial anomaly, as inferred for other propagating ridges, such as the Galapagos rift [*Sinton et al.*, 1983]. The axial positive anomaly appears to be interrupted close to the summit of the volcanic edifice, probably due to a dipole effect.

3.4. The Triple Junction Area

The BTJ is located in the area between the Bouvet southwestern RTI and the Conrad eastern RTI (Plate 1). The area is structurally very complex on a small scale, and univocal interpretations are not always possible, particularly if we reason in strictly orthodox terms of accretionary or transform boundaries separating rigid plates.

We have noted that the southernmost MAR bifurcates at its southern tip (about 54°45′S, 00°43′W) in two small branches

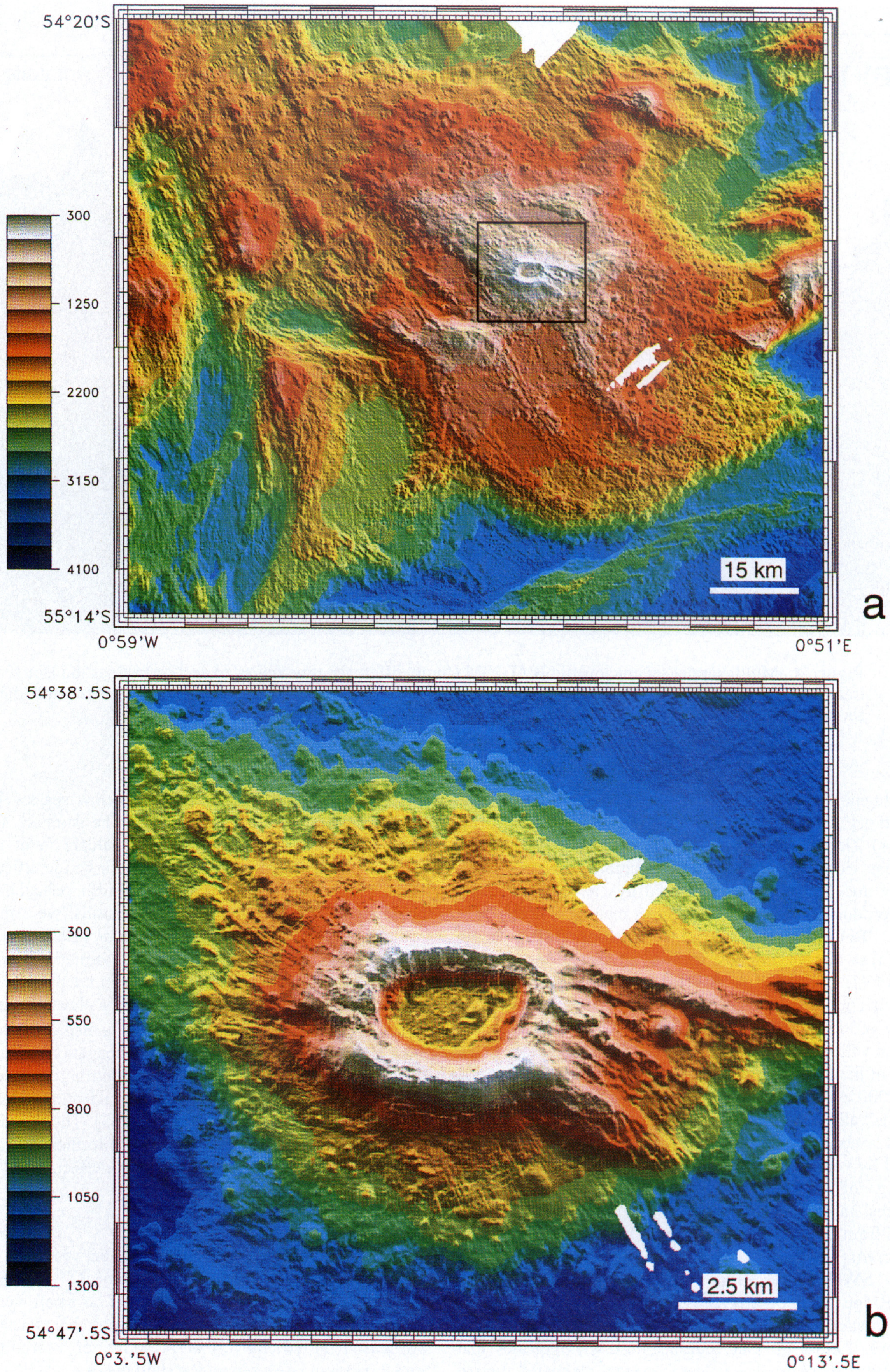

Plate 6. (a) Shaded-relief morphostructural image of the SWIR segment named Spiess Ridge and the triple junction area. Data obtained from swath bathymetry gridded using 100 m steps. (b) Zoom into the Spiess caldera. Swath bathymetry data are gridded using 25 m steps.

(Plate 6a). The bifurcation marks probably a former RRR TJ. This position for the TJ is within a few kilometers of that suggested by *Sclater et al.* [1976], although they had proposed a RFF rather than a RRR configuration. We have suggested, however, that this RRR TJ is not active at present [*Ligi et al.*, 1997].

The TJ region is characterized by three rift valleys ranging in depth between 2600 m and 3000 m (Figure 5). The northern valley, oriented 335° and corresponding to the last (southernmost) segment of the MAR, has high reflectivity [*Mitchell and Livermore*, 1998a]. Its deepest part (>2400 m) is in an asymmetric position, being close to the valley's western flank. Three small seamounts are present at the intersection of the three valleys (Figure 5).

Segment X runs south from the intersection for about 35 km, with a ~10 km wide axial valley oriented 0°. The valley has high acoustic reflectivity and is dissected by topographic lineations (probably fault scarps) also oriented 0°. However, these lineations curve to the west on the southern, deepest (3000 m) part of the valley. This deep, curving portion of the valley connects to the oblique segment of AAR through an E-W intensely deformed strike-slip zone (55°S, 1°W), involving a set of en echelon faults, frequently with sigmoidal geometry (Figure 5). These features can be interpreted as "tension gashes" within a zone subjected to sinistral shear [*Dauteuil and Brun*, 1996]. Therefore this zone is probably a 30-km-long transform offset, as supported also by the curvature of the fabric of segment X and by the deepening of its valley, which resembles a "mini" nodal basin. The 95° to 115° lineations at 55°S and 1°W, observed by *Mitchell and Livermore* [1998a], but not seen in our multibeam data, could be synthetic Riedel-Pshears [*Christie-Blick and Biddle,* 1985].

Segment Y's axial valley runs 115° for about 35 km. It is roughly 2600 m deep and shows lineations oriented between 125° and 135°. The width and depth of this valley decrease eastward; this led to the suggestion of a decrease in the net extension of this zone [*Mitchell and Livermore*, 1998a]. However, our multibeam data show that the eastern part of the valley is hidden by intense volcanism. High seafloor reflectivity is shown by MR-1 data [*Mitchell and Livermore*, 1998a, Figure 3] not only at the western part of the segment Y but also to the north of segment Y (54°42'S and 0°30'W), indicating recent volcanism along a curved belt with southward concavity. Rotated seafloor fabric can be observed (54°40'S and 0°22'W) in the boundary area between segment Y and the northern part of Spiess Ridge, to the north of the high reflectivity zone (Figure 5).

Outside the MAR bifurcation, margins A and B of the rift valley (Figure 5) have been lifted up to 1200-1400 m below sea level. Moving away from A and B, the seafloor deepens gradually, suggesting that blocks A and B are flexured due to "footwall uplift" related to the presence of normal fault planes, parallel to, and dipping toward, the axes of the two rifts. Structural high C, located between the X and Y branches (Figure 5), can be considered a "triple junction horst" [*Bahat and Mohr,* 1987] that forms an "upward triangular area" limited by two rift systems. Uplift is maximal at the northern apex of block C; it is also asymmetric, being higher at the margin of rift X, where depths (1500 m) similar to those of blocks A and B are reached.

3.4.1. Recent Evolution of the BTJ. Let us consider now how the *Mitchell and Livermore* [1998a] model of recent evolution of the BTJ differs from ours [*Ligi et al.*, 1997, and this paper]. We proposed that NW propagation of Spiess Ridge, roughly 1 Ma, "killed" the Y segment of the SWIR and de-activated a RRR triple junction, located at the bifurcation of the MAR into X (AAR) and Y (SWIR) branches. We further suggested that Spiess Ridge is propagating NW at a rate of 40 to 50 mm/yr, and we speculated that if propagation will continue at the present rate, the Spiess-SWIR ridge will impact with the MAR at roughly 54°25'S within the next 1 m.y., where a new RRR triple junction will be established.

Mitchell and Livermore [1998a,b] agree on the importance of Spiess Ridge in the evolution of the BTJ. However, they suggest that thermal weakening of the lithosphere related to the formation of Spiess Ridge at roughly 2-3 Ma triggered a diffuse boundary between the Antarctic and African plates north of the Bouvet transform. They do not believe that segment Y was a former boundary between Antarctica and Africa. They suggest instead that rift Y formed because of a clockwise change in orientation of the MAR-related stress field, due to the development of the Spiess volcanic system. However, if this change of orientation of MAR were true, we would expect evidence of compression on block A. We observe no such evidence; on the contrary, we find that A is an inclined block affected by tensional stresses and bordered by normal faults parallel to MAR and to rift X.

Mitchell and Livermore's [1998a] "radiating fabrics", with directions from 170° to 190°, were observed on horst C west of the crest, while to the east lineations oriented 130°-140° are visible (Figure 5 and their Figure 3). This observation suggests an evolution from RFF to RRR according to mechanisms proposed by *Kleinrock and Phipps Morgan* [1988], whereby in RTIs the field of shear stress related to transform motion interacts with the field of tensile stress induced by spreading. The result is a rotation of the direction of maximal tensile stress, causing the curvature of the ridge axis (MAR) toward the transforms and the bifurcation in the two new X and Y segments.

The 130°-140° fabric at 55°10'S and 0°25'W (Figure 5 and Figure 3 of *Mitchell and Livermore* [1998a]) indicates that spreading with SWIR orientation was already taking place in this area before the development of the Spiess volcanic system. This is in contrast to Mitchell and Livermore's hypothesis of an Antarctic-Africa plate boundary in the area north of the Bouvet transform developing after the formation of Spiess Ridge.

In our view, the three subparallel volcanic lineations SW of Spiess Ridge (Plate 6a and Figure 5) could represent different stages of axial magmatism, affected also by gravity stresses due to excess topography of the Spiess volcanic system (i.e., curving geometry of the three lineations).

Mitchell and Livermore [1998a,b] main objection to our hypothesis of recent (1 Ma) NW propagation of the Spiess Ridge [*Ligi et al.*, 1997] is the presence SW of Spiess of magnetic anomaly C2 interpreted by them as produced by Spiess Ridge. However, the alleged C2 magnetic anomaly SW of Spiess (54°43'S and 0°12'W) intersects the axial anomaly with a 20° to 30° angle (Plate 2 and Figure 5). Moreover, this anomaly does not have a corresponding symmetrical anomaly across the axis of Spiess Ridge, as one would expect if it had been produced by spreading from Spiess Ridge. In our view, this magnetic anomaly is not related to Spiess Ridge but was produced by a NW receding

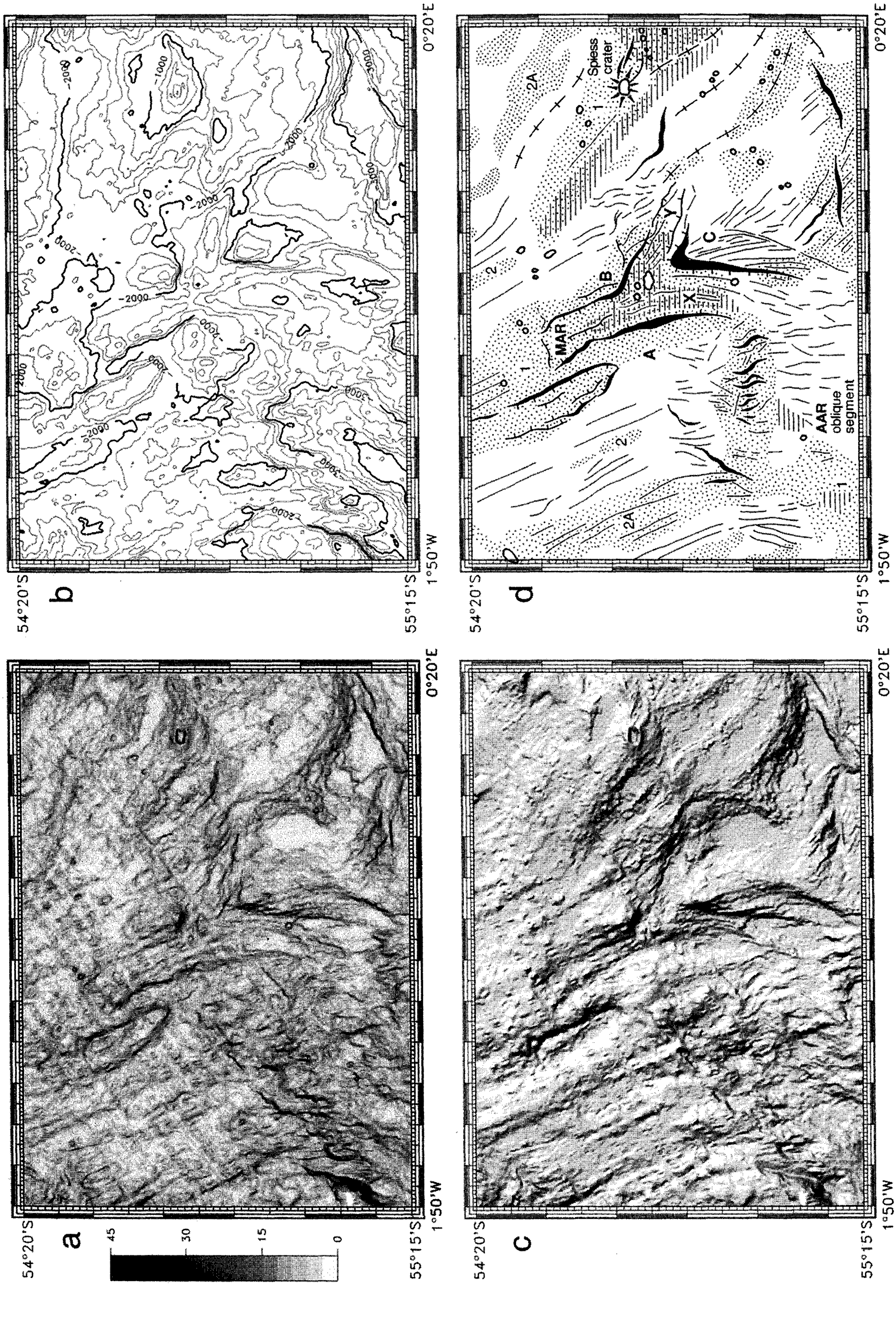
a
b
c
d
54°20'S
55°15'S
1°50'W
0°20'E
45
30
15
0
-1000
-2000
-3000
MAR
A
B
C
X
Y
Spiess crater
AAR oblique segment
2A
2
1

MAR and by development of segment Y within a RRR TJ. The presence of this magnetic anomaly and the length (35 km) of segment Y (with a rate of lengthening of 18 mm/yr) suggest roughly 2 Ma as the age when this configuration started.

The propagating Spiess segment, with its axial topographic high and a wide (30 km) zone of overlapping, shows morphology and geometry similar to those of the 87°30'W propagator on the Galapagos spreading center [*Perram and Macdonald*, 1994] but contrasting with those of the Galapagos 95°30'W propagator [*Hey et al.*, 1986] that has an axial valley and a narrow zone of overlapping. The differences of morphology and of "propagation strength" (higher at 87°30'W) between the two Galapagos propagators is probably due to a different supply of magma [*Perram and Macdonald*, 1994]. Magmatic activity is robust at the 87°30'W propagator but weak and with tectonic activity prevailing at the 95°30'W propagator. In our interpretation Spiess Ridge is a magma-rich-type propagator, similar to the 87°30'W Galapagos propagator.

3.4.2. Propagation of SWIR/Spiess Ridge. If and how the Spiess Ridge propagated is crucial to reconstruct the recent evolution of the triple junction. We outline two hypotheses.

3.4.2.1. Hypothesis (1): The outer pseudofault is marked by an E-W discontinuity of the magnetic anomalies at about 54°25'S, also where the MAR-parallel morphostructural grain starts to curve (Plates 2 and 6a). In this model the outer pseudofault makes a 38° angle with the direction of propagation (237°). Given a ~15 mm/yr spreading full rate, this geometry implies a propagation rate of 10 mm/yr. Considering that the propagating Spiess segment is ~50 km long, it would follow that propagation started at about 5 Ma.

A RRF configuration could be assumed before this time (Figure 6); this configuration is unstable if we assume orthogonal and symmetric spreading (as in *McKenzie and Morgan* [1969]); it can be stable if we assume asymmetric and/or oblique spreading (as in *Patriat and Courtillot* [1984]). If Spiess Ridge started propagating at 5 Ma, the tip of MAR receded while repeatedly curving outward (N-S). The AAR segment lengthened north, but by 3.5 Ma it was no longer linked with MAR except by a 30-km-long transform.

This hypothesis runs into difficulties. Not enough crust has been produced on the western side of both the propagating SWIR segment and the receding MAR segment, unless strongly asymmetric spreading is assumed for both. However, we note only a weak asymmetry in SWIR spreading next to Bouvet island and a very weak asymmetry for segments of MAR during the chron 2A to chron 3A time interval (2.6-5.9 Ma according to *Huestis and Acton* [1997]). Moreover, we do not observe a large shear or transform zone between the propagating SWIR and the receding MAR, but instead, we observe rift Y cutting through overlapped crust.

3.4.2.2. Hypothesis 2: This hypothesis was briefly outlined by *Ligi et al.* [1997]. The outer and inner pseudofaults are marked by topographic depressions adjacent to the axial topographic high of the propagating segment. On the "inner side", the negative magnetic anomaly adjacent and subparallel to the axial anomaly (Plates 2, 5 and Figure 7) was produced by the propagating Spiess Ridge. The small positive anomaly next to it makes a 20°-30° angle β with the central anomaly. It is probably anomaly C2, produced in part by the Y segment of the SWIR and partly by the NW receding MAR. Given the expression $w = u/\tan\alpha$ [*Shoeberg and Stein*, 1994] and assuming a half spreading rate u of 7.25 mm/yr, the angle ~10° α of the pseudofaults relative to the direction of propagation indicates a rate of propagation w of 40 to 50 mm/yr.

The propagating tip is presently located at about 54°25'S, 0°32'W (Plate 6a and Figure 5). We assume that the initial source of the propagator was at the present site of minimum depth of the Spiess volcanic system, i.e., where the emplacement of magma has been maximal. This site is located roughly 50 km SE of the propagating tip, a distance that can be covered in ~1 m.y. at the estimated rate of propagation. Accordingly, we suggest that the igneous event that gave rise to the new SWIR-Spiess segment started at roughly 1 Ma, consistently with the observation that the oldest magnetic anomalies produced by Spiess Ridge are within the Matuyama epoch.

An independent estimate of the rate of propagation can be obtained from a model of *Morgan and Parmentier* [1985] where propagation is driven by stresses induced by gravity at the rift tip, caused by isostatically compensated excess topography of the propagating ridge. The rift propagates if a "stress intensity factor" k at the rift tip exceeds a threshold value. The rift is equated to a crack or conduit in the lithosphere; the forces resisting propagation are related to the distribution of pressure within the crack. The stress intensity factor related to the resisting forces can be estimated from

$$k_r = \mu H^{3/2}(9w+11.25u)/d^2 \tag{1}$$

where μ is viscosity, H is thickness of the lithosphere, d is width of the conduit, w is rate of propagation and u is half spreading rate. Assuming $\mu = 2\times10^{18}$ Pa s, H=d=10 km, w=40.4, and u=7.25 mm/yr, from (1) we obtain k_r=0.2819x10^9 Pa m$^{1/2}$. The forces that drive propagation, and those that resist it, determine the topography of the propagating rift. Following *Morgan and Parmentier* [1985], we calculated the total stress intensity factor K=($k_d + k_r$) using

Figure 5. Triple junction area. (a) Map of maximum topographic slopes. Shaded bar is in degrees of topographic slope. The topographic gradient was computed along eight different directions at each node of the bathymetric grid. The plotted slope corresponds to the maximum gradient. (b) Bathymetry. Contour interval is 200 m. (c) Shaded relief map. Illumination is from NE with an elevation of 45° above the horizon. (d) Structural sketch map based on a joint interpretation of Hawaii-MR1 side-scan sonar [*Mitchell and Livermore*, 1998a, b] and our multibeam and magnetic data. Horizontal solid line patterns represent high backscatter of *Mitchell and Livermore* [1998a, b]. The positive magnetic anomalies are indicated with dotted patterns and magnetic chron indications are overprinted. Thin solid lines, oceanic fabric; thick solid lines with hatches, normal faults. The alternating bands with different roughness striking SW-NE in the northwestern sector of Figures 5a and 5c corresponds to interpolation artifacts between ship tracks related to incomplete coverage between adjacent multibeam swaths during the 1994 cruise.

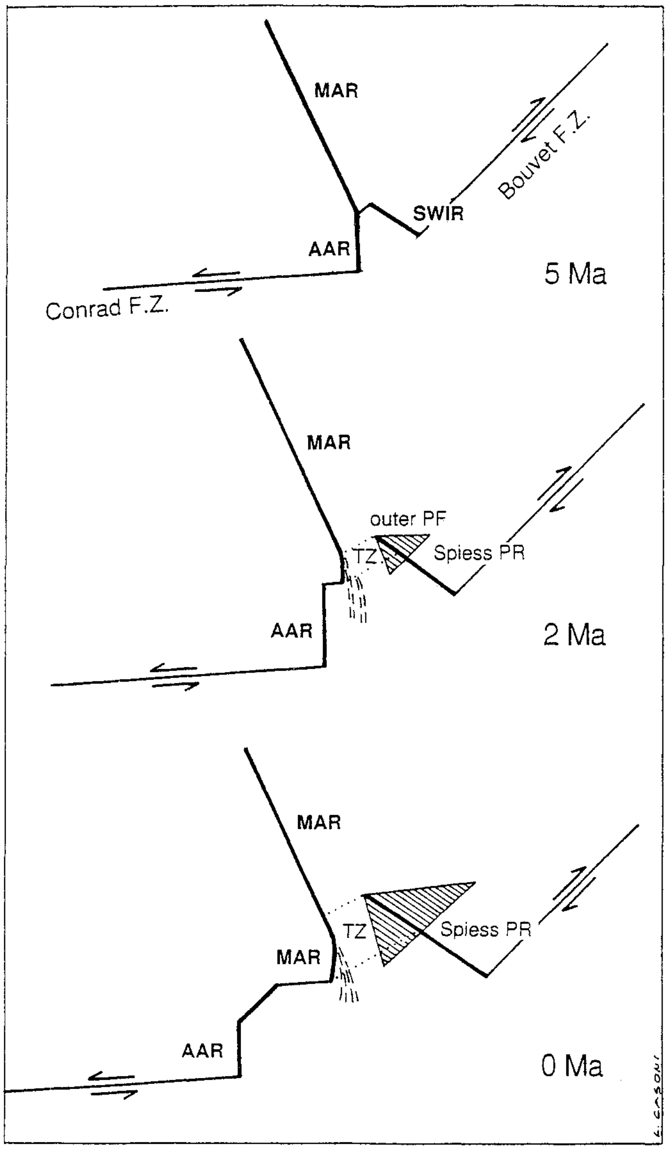

Figure 6. Cartoon of the recent Bouvet Triple Junction evolution assuming that Spiess propagation started at 5 Ma (hypothesis 1). This hypothesis runs into difficulties because not enough crust has been produced between the propagating SWIR and the receding MAR segment, and we do not observe a large shear or transform zone but instead, observe rift Y cutting through overlapped crust. TZ, transform zone; double dashed line, failed MAR segment; hatched pattern, crust produced by Spiess propagating segment.

a linear approximation $\delta(x)$ of the residual topographic anomaly between the axial profile of Spiess Ridge and a parallel profile located 10 km from this axis (Figure 8), where k_d and k_r represent the positive and the negative contributions respectively to the stress intensity factor. Given that the length of the Spiess propagating segment is 46 km, we obtained k_d=0.5625x10^9 Pa m$^{1/2}$ and k_r=0.2819x10^9 Pa m$^{1/2}$. The negative contribution is due to those dynamic forces opposing propagation. Comparing the value for k_r with that computed from (1), we obtain a propagation rate of 40 mm/yr, a value close to that estimated from the observed angle of the propagating rift with the V-shaped pseudofaults.

This agreement notwithstanding, the application of *Morgan and Parmentier*'s [1985] model to the propagation of Spiess Ridge runs into some problems. A fall of pressure in the asthenospheric viscous flux is expected at the tip of the propagator, producing a dynamically supported axial topographic depression, as observed near the tip of the Galapagos 95°30'W propagator [*Searle and Hey*, 1983; *Hey et al.*, 1986; *Kleinrock and Hey*, 1989; *Kleinrock et al.*, 1989]. Gravimetry suggests that this topography is indeed dynamically supported [*Morgan and Parmentier*, 1987]. However, the axial morphology of the Spiess propagator is different from that of the 95°30'W Galapagos propagator. The Spiess axial profile is "swollen" and has a broad overlapping zone with the receding rift (branch Y in Plate 2), in contrast with the axial depression and the small overlapping zone at the 95°30'W Galapagos propagator. These differences may be due to a different supply of magma in the two cases. The presence of magma in the crack may decrease the critical stress intensity factor necessary in order for propagation to take place [*Rubin and Pollard*, 1988], thus affecting the rate of propagation and the size of the overlap zone.

The abundance of magmatic activity and the lack of an axial rift valley for the propagating Spiess Ridge suggest that the viscous forces in the conduit are not sufficient to prevent propagation. The large supply of magma may be the cause of the high rate of propagation, roughly 5 times the rate of spreading. Propagators with velocities 1-3 times higher than the spreading rate have been observed along the MAR [*Kleinrock et al.*, 1997], where, however, the high speed of propagation has been related to stages of tectonic extension alternating with periods of magmatic injection along the ridge axis.

According to our hypothesis the configuration of the TJ prior to 1 Ma was of RRR type, with AAR and SWIR being connected to MAR through segments X and Y, respectively (TJ1 in Figure 7). Segment Y was abandoned at a speed lower than the rate of propagation of Spiess Ridge, which would explain the slight outward curvature of the abandoned segment. On the other hand, the southernmost segments of MAR continued to produce spreading crust after 1 Ma.

The production of crust by both the Spiess propagating segment and MAR would cause a limited "internal" sheared zone. We suggest, however, that the excess crust creates also an "external" (sinistral) sheared zone (Plate 5b) with the deformation being transferred to the adjacent Bouvet transform plate boundary. The northern boundary of the external sheared zone is a E-W lineation at 54°25'S; the southern boundary is the fracture zone created by the former transform offset between segment Y and Spiess segment. Excess crust formation at Spiess Ridge and MAR could be the ultimate cause of the extensional brittle deformation in the extended zone. This hypothesis is compatible with the suggestion that extension on the northern side of the Bouvet transform is due to the angle between the transform and the direction of motion of the African plate [*Mitchell et al.*, 1997]. It would also explain, however, why deformation is not limited to the vicinity of the transform plate boundary but is, in fact, maximal well away from the boundary.

4. Evolution of the Bouvet Triple Junction

The geometry and stability of a TJ are related to the relative velocities of the three plates and to the orientation of the three

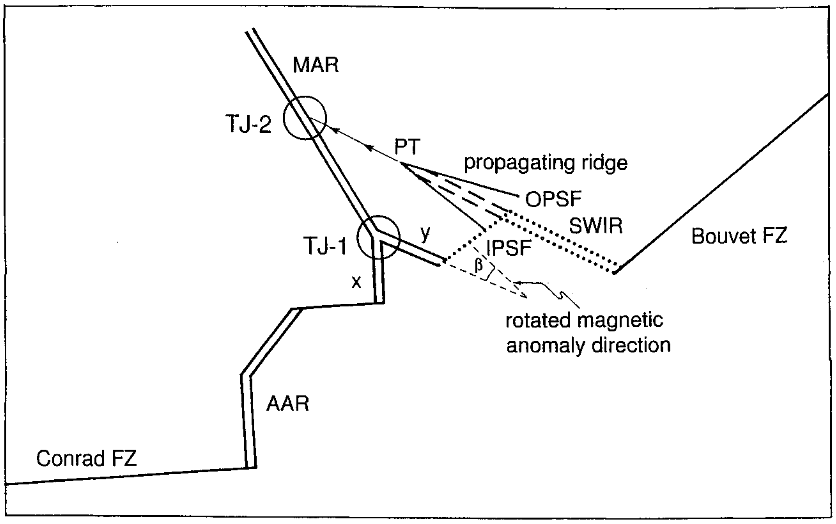

Figure 7. Scheme outlining the Bouvet Triple Junction evolution, including a predicted configuration about 1 m.y. in the future, assuming that Spiess propagation started at 1 Ma (hypothesis 2). The present configuration implies that TJ1 is inactive because the SWIR-Spiess propagating segment has disrupted the RRR (TJ1) configuration. PT, tip of the SWIR-Spiess propagating ridge; IPSF, inner pseudofaults; OPSF, outer pseudofaults. The predicted future RRR configuration TJ2 will be established within the forthcoming 1 m.y.

plate boundaries at their meeting point [*McKenzie and Morgan*, 1969]. Any perturbation of spreading rate and/or orientation of the plate boundaries can affect the stability of a TJ and force a change in its configuration.

The BTJ has in the past shifted repeatedly from RFF to RRR and vice versa, as suggested by Plate 1 where AAR and SWIR display coupled transforms joined by short ridge segments. If we assume symmetrical and orthogonal spreading, conditions of stability are more restricted for a RFF junction than for a RRR junction [*McKenzie and Morgan*, 1969] because the velocity triangle must be isosceles in order to have stability; that is, two of the three ridges must have the same spreading rate. If the velocity triangle is not isosceles, stability of a RFF junction can be achieved only if the nontransform boundary has asymmetric or oblique spreading [*Johnson et al.*, 1973; *Patriat and Courtillot*, 1984]. Thus the different spreading rates of AAR and SWIR must be compensated by asymmetric or oblique spreading of MAR.

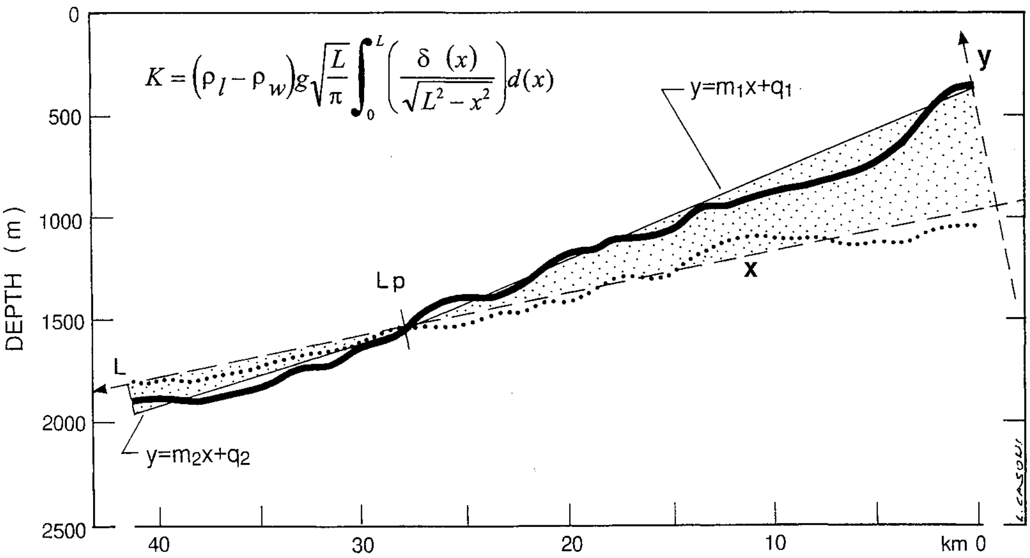

Figure 8. Ridge axis topography for the SWIR-Spiess propagating ridge, thick solid line; 10 km off-axis profile, thick dotted line; linearized Spiess Ridge topographic anomaly $\delta(x)$ (m_1=-0.02102, q_1=620 m, m_2=-0.01091 and q_2=321.82 m) obtained by the difference between the ridge axis and off-axis seafloor elevation, used to calculate a stress intensity factor following *Morgan and Parmentier* [1985], thin solid line. L_p marks the abscissa bounding positive and negative contributions to the stress intensity factor k. The ρ_l and ρ_w are density of the lithosphere (3300 kg/m^3) and density of water (1000 kg/m^3), respectively; $2L$ is length of the conduit; g is acceleration of gravity (9.780 m/s^2).

Spreading full rates derived from magnetic anomalies are: 30.5 mm/yr up to chron 4A (~9 Ma) for the MAR segment close to the BTJ; 19.5 mm/yr up to chron 4 (~8 Ma) for the AAR segment north of the Conrad transform; and 14.5 mm/yr up to chron 2A (~3 Ma) for the SWIR segment east of Bouvet island (Figure 2). These values are close to those estimated from the global plate motion model NUVEL-1A [*DeMets et al.*, 1994] assuming the present position of BTJ for the last 3 m.y., i.e., 29.5, 17.8, and 13.4 mm/yr for MAR, AAR, and SWIR, respectively. Model NUVEL of *DeMets et al.* [1990, 1994] has significantly reduced systematic misfits of some spreading rates compared to previous models. However, NUVEL gives spreading rates lower by 1-2 mm/yr than those observed for Antarctica-South America and Africa-Antarctica plate motion due to nonclosure of this three plate circuit. Nonclosure about the BTJ may be caused by systematic errors or may reflect intraplate deformation [*DeMets et al.*, 1990; *Gordon*, 1995]. Given the uncertainty at the BTJ of global plate motion models and given that the velocity triangle obtained from our magnetic data (inset in Plate 2) agrees well with the observed geometry at TJ-1 (Figure 7), we assume the relative velocities cited above in describing the recent evolution of the BTJ (Figure 9). Morphology and magnetics suggest the following evolution of the BTJ since 10 Ma (chron 5), when the MAR extended south up to the Conrad and Bouvet transforms in a RFF configuration.

The MAR lengthened southward (Antarctica reference frame) within a RFF configuration (MAR plus Bouvet and Conrad transforms), while the two transforms increased their offset length at the AAR and SWIR spreading half rate [*Patriat and Courtillot*, 1984; *Apotria and Gray*, 1985]. Assuming that the Conrad and Bouvet transforms represent a period of stable RFF configuration prior to chron 5, for the AAR we estimate an average spreading full rate of 26 mm/yr during the chron 8 to chron 5 time interval (25.9-9.9 Ma according to *Huestis and Acton* [1997]), utilizing the South America-Antarctica rotation parameters of *Barker and Lawver* [1988]. Given that the Conrad transform is ~200 km long, we estimate that roughly 15 m.y. are required for its development. We assume therefore that the BTJ had a stable RFF configuration starting from ~25 Ma up to roughly 10 Ma (Figure 10), when it changed into a RRR configuration, probably due to a change in relative velocities and a consequent shift from conditions of stability .

The transition from RFF to RRR probably did not take place through a bifurcation of the MAR [*Kleinrock and Phipps Morgan*, 1988] but through an intermediate unstable RRF configuration, which lasted at least 1 m.y. During this configuration, perhaps favored by a slight asymmetry in the spreading of SWIR and MAR, the TJ migrated westward, while the last AAR segment developed. The SWIR (pre-Spiess) segment developed at ~9 Ma, when the TJ changed

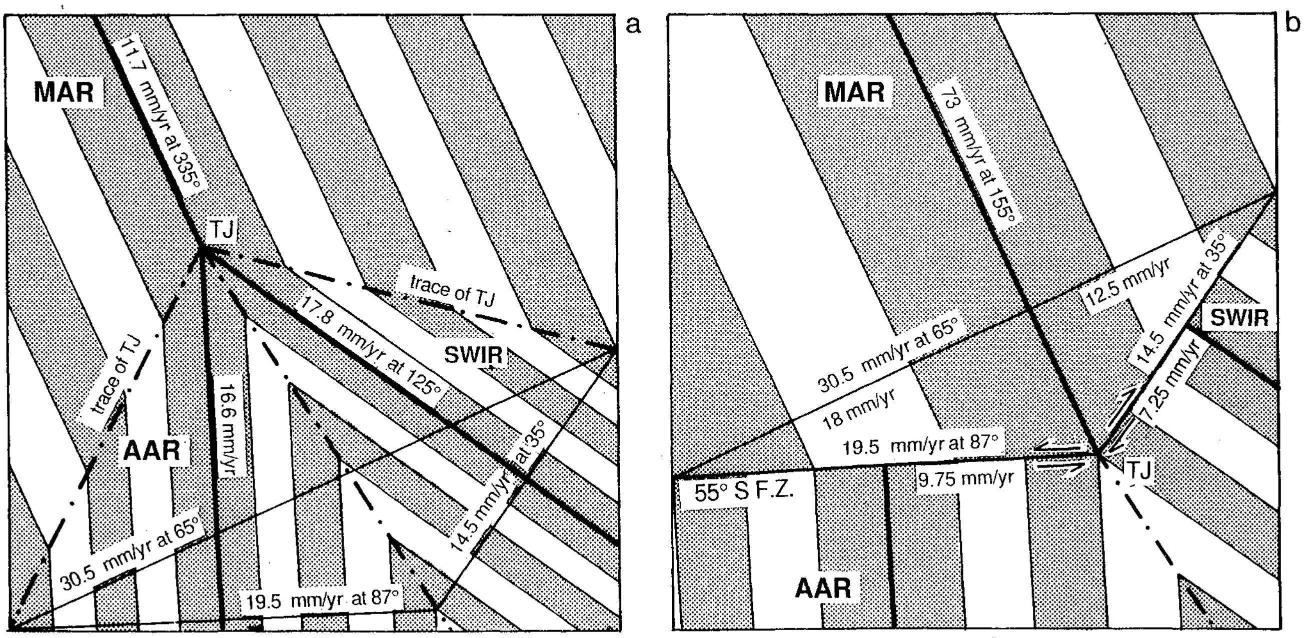

Figure 9. The velocity triangle for the Bouvet Triple Junction was compatible in the past both with a RFF and RRR configuration [*Sclater et al.*, 1976]. Conditions of stability for RFF are more restricted than those for a RRR junction because the velocity triangle must be isosceles assuming symmetrical and orthogonal spreading. Stability can be achieved with a nonisosceles velocity triangle, assuming asymmetric or oblique spreading of the nontransform boundary. (a) The present velocity triangle for Bouvet TJ compatible with RRR configuration under assumption of orthogonal and symmetrical spreading. In this RRR mode, MAR recedes by 11.7 mm/yr and AAR and SWIR lengthen by 16.6 and 17.8 mm/yr, respectively. (b) The present velocity triangle for Bouvet TJ compatible with RFF configuration under assumption of orthogonal and asymmetric spreading. The different spreading rates of AAR and SWIR are compensated by asymmetric spreading of MAR. In this RFF mode, MAR lengthens by 7.3 mm/yr, while the two transforms increase their offset length at the AAR and SWIR spreading half rate (9.75 and 7.25 mm/yr, respectively, assuming symmetric spreading).

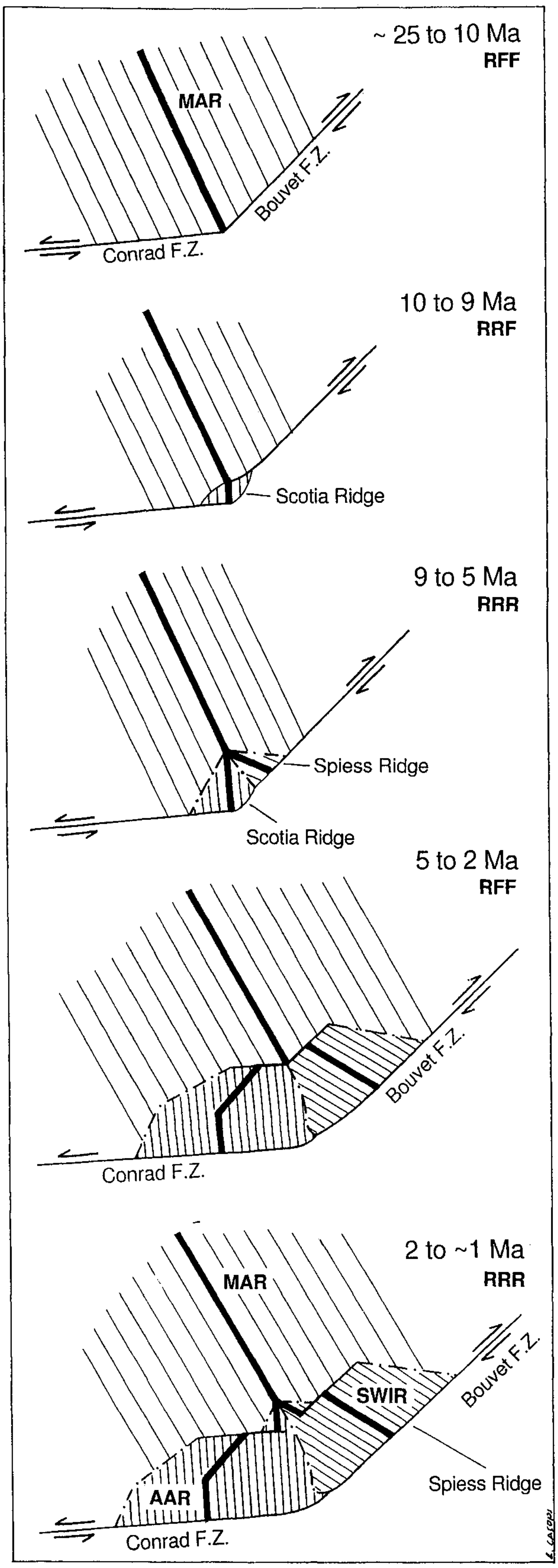

Figure 10. Cartoon showing the Bouvet Triple Junction evolution from ~25 Ma to Recent. Hatched patterns with different orientations mark crust produced by different ridge segments. For furher explanations, see text.

into a RRR configuration that lasted up to ~5 Ma. During this time interval, assuming the Antarctic plate as fixed, the MAR receded NNW, while the AAR (Scotia Ridge) and the SWIR (Spiess Ridge) increased their length at rates of 16.6 and 17.8 mm/yr, respectively (Figure 9a).

During this interval of RRR evolution the AAR segment developed obliquely to the spreading direction, perhaps due to a decreased supply of magma from the mantle. The oblique AAR segment is presently characterized by nearly amagmatic extension, although morphology and acoustic reflectivity suggest the presence within the oblique trough of small en echelon N-S zones of accretion. The presence of other oblique AAR segments (Plate 1) suggests that episodes of magma starvation at the AAR may have resulted in instability of the RRR configuration leading to periods with RFF geometry. A transition from RRR to RFF occurred ~5 Ma, leading to the development of two small transforms. The RFF configuration (Figure 9b) lasted about 3 m.y. (as estimated from the ~30 km length of these transforms) and was favored by a weak asymmetry of spreading of the MAR (Figures 2a and 2b, interval C2A-C3A). The MAR southern tip bifurcated in two branches (X and Y in Plate 2), and the BTJ became again RRR at roughly 2 Ma (Figure 10), given the ~35 km lengths and lengthening velocities of the two ridges.

The recent instability has been caused by an intense thermal/magmatic event that, coupled with a low spreading rate, has determined the swollen topography of the SWIR-Spiess segment, the filling up of the southwestern part of the Bouvet transform valley, and the flooding of preexisting crust with obliteration of magnetic anomalies. Forces related to the excess of axial topography caused NW propagation of the SWIR-Spiess Ridge into the African plate, determining the abandonment of segment Y and the destruction of the RRR configuration. It follows that at present the BTJ is not represented by a triple point but by a zone of deformation located between the propagating and the receding segments (Figure 7).

If the SWIR-Spiess segment will continue its propagation NW at the estimated rate of 40-50 mm/yr, we can estimate that it will intersect the MAR within <1 m.y. at about 54°25'S, 1°10'W (TJ2 in Figure 7). This would create a new RRR BTJ, with a ~70 km long stretch of MAR being captured by the AAR and with a significant enlargement of the Antarctic plate.

5. Conclusions

The BTJ region is characterized in general by (1) small-scale variability in space and time of the position of the accretionary and transform plate boundaries; (2) a complex evolution in time of the geometry and structural configuration (either RRR or RFF) of the triple junction; (3) anomalous swelling of the topography of two (MAR and SWIR) of the three accretionary boundaries, related to melting anomalies below the Spiess-SWIR volcanic system, the intraplate Bouvet island, and portions of the MAR.

5.1. Variability of the Accretionary Plate Boundaries

Ridge jumping, ridge overlapping, and ridge propagation are not common in slow spreading ridges. However, our results show that they are unusually common in the BTJ region, notwithstanding the relatively low (MAR) or very low

(SWIR, AAR) spreading rates. This unstable geometry of the plate boundaries probably derives from the combination of two factors. One is the complex and variable distribution of stresses in the region due to the meeting of three major plates. The other, which appears to be valid at least for the MAR and SWIR, is the seemingly high (although variable) rate of magma supply from the mantle relative to spreading rate, which results in magmatic pulses in zones of least strength, triggering swelling of the igneous crustal layer and ridge propagation or jumping.

5.2. Evolution of the Bouvet Triple Junction

During the last 25 m.y. the BTJ has shifted repeatedly from RFF to RRR configurations and vice versa. The BTJ had a stable RFF configuration from roughly 25 Ma to roughly 10 Ma, when the MAR lengthened southward and the Conrad and Bouvet transforms increased their offset length. The BTJ shifted to a RRR configuration at roughly 10 Ma, probably due to changes in the relative spreading rates, with a short-lived, unstable RRF stage in between. During this RRR stage, that lasted up to ~5 m.y., the MAR receded NNW, while the last segments of the AAR and SWIR increased their length. A shift from a RRR to a RFF geometry took place at roughly 5 Ma, with the development of two small transforms at the tip of the MAR. At about 2 Ma the southern tip of the MAR bifurcated in two small branches, so that a RRR configuration prevailed again. One of the two branches became inactive at roughly 1 Ma due to the SWIR-Spiess magmatic event. Therefore the present-day BTJ is not a triple point, but an is area of diffuse deformation. A new RRR BTJ might be established at ~54°30'S, 1°10'W in about 1 m.y., when the propagating SWIR/Spiess segment will impact with the MAR. A ~70-km-long portion of MAR will then be captured by the AAR, and the Antarctic plate will grow [*Ligi et al.*, 1997].

5.3. Melting Anomalies in the Bouvet Region

The depth anomalies in the southern segments of the MAR, in the SWIR segment adjacent to the Bouvet island, in Bouvet island itself, and in the SWIR-Spiess Ridge, all support the hypothesis that excess melting in the mantle is widespread in the region. In contrast, the AAR is deeper than "normal".

5.3.1. Bouvet Island. The largest melting anomaly is that of Bouvet island, which is widely considered as the site of a mantle plume or hot spot [*Morgan*, 1972; *Le Roex*, 1987; *Kurz et al.*, 1998]. Recent volcanic activity has taken place in the island [*Baker and Tomblin*, 1964]. The swelling of the SWIR segment adjacent to Bouvet island is clearly caused by the same melting anomaly responsible for the excess volcanism that gave rise to the island. MORB from this segment has relatively low Na_8 and high H_2O and LREE contents, suggesting a high degree of melting of a source containing a LREE and volatile enriched component, compatible with a significant influence from the Bouvet hot spot [*Simonov et al.*, 1996].

5.3.2. Spiess Ridge. The Spiess Ridge constitutes another major melting anomaly. It is not clear whether the melt is compatible with a Bouvet hot spot source [*Le Roex et al.*, 1982; *Le Roex*, 1987; *Simonov et al.*, 1996; *Kurz et al.*, 1998]. The elevated topography of Spiess Ridge is the result of an unusually high rate of magma supply relative to the low spreading rate (14.5 mm/yr). When spreading cannot keep up with an overabundant magma supply, the basaltic crust thickens and the topography swells [*Morgan and Chen*, 1993], triggering propagation.

5.3.3. MAR Southernmost Segments. Swelled stretches of the MAR between the Agulhas Fracture Zone (FZ) and 53°S have been attributed to the influence on the MAR of the Discovery and Shona hot spots [*Douglass et al.*, 1995; *Small*, 1995]. The MAR south of 53°S also shows positive topographic anomalies. Their significance will be clarified after completion of elemental and isotopic analyses of basaltic glasses collected by us from this stretch of MAR.

The occurrence of melting anomalies in the Bouvet region may indicate a widespread regional distribution of thermal anomalies in the upper mantle. These thermal anomalies affect strongly the characteristics of two of the three plate boundaries that converge into the BTJ and cause "active" rather than "passive" formation of oceanic crust in significant portions of these boundaries. These anomalies also affect the evolution in space and time of the BTJ. Whether or not this hotter than normal mantle is related to the presence of the triple junction itself is a matter of debate. Several other triple junctions (i.e., Easter, Afar) appear to be associated with hot spots or unusually hot mantle. However, at least another major TJ, i.e., the Rodriguez TJ in the Indian Ocean, does not appear to be associated with an unusually hot upper mantle [*Munschy and Schlich*, 1989].

Acknowledgments. The field work was sponsored by the Italian Antarctic Project (PNRA) and the post-cruise research was sponsored by "Progetto Strategico Dorsali Oceaniche" of the Italian CNR. This project is the result of a cooperation between the Istituto di Geologia Marina, CNR, Bologna, and the Geology Institute of the Russian Academy of Sciences, Moscow. The Russian part was sponsored by grant RFFI-N97-05-64737. We are grateful to the officers and crews of the R/V *Strakhov* and R/V *Gelendzhik* for their skill and cooperation at sea, often under difficult weather conditions. We thank A. Argnani, F. Bertozzi, D. Brunelli, L.Casoni, A. Cipriani, L. Gasperini, D. Penitenti, F. Sciuto, C. Small, M. Terenzoni, and N. Zitellini for help during various stages of this work; R. Livermore and N. Mitchell for providing Hawaii-MR-I side-scan data and for helpful discussions. We are grateful to anonymous referees and to the associate editor K.E. Louden for help in improving the paper. Contributions N°1170 from IGM, and N°5959 from LDEO.

References

Apotria, T.G., and N.H. Gray, Absolute motion and evolution of the Bouvet Triple Junction, *Nature, 316*, 623-625, 1985.

Bahat, D. and P. Mohr, Horst faulting in continental rifts, *Tectonophysics*, 141, 61-73, 1987.

Baker, P.E., and J.F. Tomblin, A recent volcanic eruption on Bouvetoya, South Atlantic Ocean, *Nature, 203*, 1055-1056, 1964.

Barker, P.F., and L.A. Lawver, South American-Antarctic plate motion over the past 50 Myr, and the evolution of the South American-Antarctic ridge, *Geophys. J., 94*, 377-386, 1988.

Christie-Blick, N.H., and K.T. Biddle, Deformation and basin formation along strike-slip faults, in *Strike Slip Deformation, Basin Formation and Sedimentation*, edited by K.T.Biddle K. and N.Christie-Blick., *Soc. Econom. Paleontol. Mineral. Spec. Pub., 37*, 1-34, 1985.

Dauteuil, O., and J.P. Brun, Deformation partitioning in a slow spreading ridge undergoing oblique extension: Mohns Ridge, Norwegian Sea, *Tectonics, 15*, 870-884, 1996.

DeMets, C., R.G. Gordon, D.F. Argus, and S. Stein, Current plate motions, *Geophys. J. Int., 101*, 425-478, 1990.

DeMets, C., R.G. Gordon, D.F. Argus, and S. Stein, Effect of recent revisions to the geomagnetic reversal timescale on estimates of current plate motion, *Geophys. Res. Lett., 21*, 2191-2194, 1994.

Douglass, J., J.G. Schilling, R.H. Kingsley, and C. Small, Influence of the Discovery and Shona mantle plumes on the southern Mid-Atlantic Ridge: Rare earth evidence, *Geophys. Res. Lett.*, *22*, 2893-2896, 1995.

Eittreim, S., and J. Ewing, Vema fracture zone transform fault, *Geology*, *3*, 555-558, 1975.

Forsyth, D.W., Fault plane solutions and tectonics of the South Atlantic and Scotia Sea, *J. Geophys. Res.*, *80*, 1429-1443, 1975.

Gordon, R.G., Plate motions, crustal and lithospheric mobility, and paleomagnetism: Prospective viewpoint, *J. Geophys. Res.*, *100*, 24,367-24,392, 1995.

Hey, R.N., F.K. Duennebier, and W.J. Morgan, Propagating rifts on mid-ocean ridges, *J.Geophys. Res.*, *85*, 2647-2658, 1980.

Hey, R.N., M.C. Kleinrock, S.P. Miller, T.M. Atwater, and R.C. Searle, Sea Beam/Deep-Tow investigation of an active oceanic propagating rift system, Galapagos 95.5°W, *J. Geophys. Res.*, *91*, 3369-3393, 1986.

Huestis, S.P., and G.D. Acton, On the construction of geomagnetic timescales from non-prejudicial treatment of magnetic anomaly data from multiple ridges, *Geophys. J. Int.*, *129*, 176-182, 1997.

Johnson, G.L., K.N. Hey, and A. Lowrie, Marine geology in the environs of Bouvet Island and the south Atlantic Triple Junction, *Mar. Geophys. Res.*, *2*, 23-36, 1973.

Kleinrock, M.C., and R.N. Hey, Migrating transform zone and lithospheric transfer at the Galapagos 95.5°W propagator, *J. Geophys. Res.*, *94*, 13,859-13,878, 1989.

Kleinrock, M.C., and J. Phipps Morgan, triple junction reorganization, *J. Geophys. Res.*, *93*, 2981-2996, 1988.

Kleinrock, M.C., R.C. Searle, and R.N. Hey, Tectonics of the failing spreading system associated with the 95.5°W Galapagos propagator, *J. Geophys. Res.*, *94*, 13,839-13,857, 1989.

Kleinrock, M.C., B.E. Tucholke, J. Lin, and M.A. Tivey, Fast rift propagation at a slow-spreading ridge, *Geology*, *25*, 639-642, 1997.

Kurz, M.D., A.P. Le Roex, and H.J.B. Dick, Isotope geochemistry of the oceanic mantle near the Bouvet triple junction, *Geochim. Cosmochim. Acta*, *62*, 841-852, 1998.

Lawver, L. A., and H.J.B. Dick, The American Antarctic Ridge, *J. Geophys. Res.*, *88*, 8193-8202, 1983.

Le Roex, A.P., Crust-mantle evolution in the vicinity of the Bouvet Triple Junction, A synthesis, *S. Afr. J. Antarc. Res.*, *17*, 90-104, 1987.

Le Roex, A.P., H.J.B. Dick, A.M. Reid, and A.J. Erlank, Ferrobasalt from the Spiess Ridge segment of the Southwest Indian Ridge, *Earth Planet. Sci. Lett.*, *60*, 437-451, 1982.

Ligi, M., and G. Bortoluzzi, Plotmap, geophysical and geological application of good standard quality cartographic software, *Comput. and Geosci.*, *15*, 519-585, 1989.

Ligi, M., E. Bonatti, G. Bortoluzzi, G. Carrara, P. Fabretti, D. Penitenti, D. Gilod, A.A Peyve, S. Skolotnev, and N. Turko, Death and transfiguration of a triple junction in the South Atlantic, *Science*, *276*, 243-246, 1997.

Macdonald, K.C., and P.J. Fox, Overlapping spreading centers, new accretion geometry on the East Pacific Rise, *Nature*, *302*, 55-57, 1983.

McKenzie, D., The geometry of propagating rifts, *Earth Planet. Sci. Lett.*, *77*, 176-186, 1986.

McKenzie, D., and W. J. Morgan, Evolution of triple junctions, *Nature*, *224*, 125-133, 1969.

Mitchell, N.C., and R.A. Livermore, The present configuration of the Bouvet Triple Junction, *Geology*, *26*, 267-270, 1998a.

Mitchell, N.C., and R.A. Livermore, Spiess Ridge: An axial high on the slow spreading Southwest Indian Ridge, *J. Geophys. Res.*, *103*, 15,457-15,471, 1998b.

Mitchell, N.C., R.A. Livermore, R. Larter, M. Ligi, F. Martinez, A. Nankivell, and Y. Nogi, Sonar mapping of an axial high at a slow spreading ridge, Spiess Ridge at the Bouvet Triple Junction, *InterRidge News*, *4*(1), 23, 1995.

Mitchell, N.C., R.A. Livermore, and S.M. Lee, Extensive oblique faulting adjacent to the Conrad and Bouvet F.Z. near the Bouvet Triple Junction, EGS XXII General Assembly, Vienna, Australia, 21-25 April 1997, *Ann. Geophys.*, suppl. I, *15*, 164, 1997.

Morgan, P.J., and Y.S. Chen, Dependence of ridge-axis morphology on magma supply and spreading rate, *Nature*, *364*, 706-708, 1993.

Morgan, P.J., and E.M. Parmentier, Causes and rate-limiting mechanisms of ridge propagation: A fracture mechanics model, *J. Geophys. Res.*, *90*, 8603-8612, 1985.

Morgan, P.J., and E.M. Parmentier, A three-dimensional gravity study of the 95.5°W propagating rift in the Galapagos spreading center, *Earth Planet. Sci. Lett.*, *81*, 289-298, 1987.

Morgan, W.J., Deep mantle convection plumes and plate motions, *Bull. Amer. Assoc. Petrol. Geol.*, *56*, 203-213, 1972.

Munschy, M., and R. Schlich, The Rodriguez Triple Junction (Indian Ocean): Structure and evolution for the past one million years, *Mar. Geophys. Res.*, *11*, 1-14, 1989.

Patriat, P., and V. Courtillot, On the stability of triple junctions and its relation to episodicity in spreading, *Tectonics*, *3*, 317-332, 1984.

Perram, L.J., and K.C. Macdonald, An overlapping propagating spreading center at 87°30'W on the Galapagos spreading center, *Earth Planet. Sci. Lett.*, *121*, 195-211, 1994.

Rubin, A.M., and D.D. Pollard, Dike induced faulting in rift zones of Iceland and Afar, *Geology*, *16*, 413-417, 1988.

Sandwell, D.T., and W.H.F. Smith, Marine gravity anomaly from Geosat and ERS-1 satellite altimetry, *J. Geophys. Res.*, *102*, 10,039-10,054, 1997.

Sclater, J.G., C. Bowin, R. Hey, H. Hoskins, J. Peirce, J. Philips, and C. Tapscott, The Bouvet Triple Junction, *J. Geophys. Res.*, *81*, 1857-1869, 1976.

Sclater, J.G., H.J.B. Dick, I.O. Norton, and D. Woodroffe, Tectonic structure and petrology of the Antarctic plate boundary near the Bouvet Triple Junction, *Earth Planet. Sci. Lett.*, *37*, 393-400, 1978.

Searle, R.C., and R.N. Hey, GLORIA observations of the propagating rift at 95.5°W on the Cocos-Nazca spreading center, *J. Geophys. Res.*, *88*, 6433-6447, 1983.

Shoeberg, T., and S. Stein, Investigation of spreading center evolution by inversion of seafloor magnetic anomaly and tectonic fabric data, *Earth Planet. Sci. Lett.*, *122*, 195-202, 1994.

Simonov, S., A.A. Peyve, V.Y. Kobolov, A.A. Milonosov, and S.V. Kovyazin, Magmatic and hydrothermal processes in the Bouvet Triple Junction region (South Atlantic), *Terra Nova*, *8*, 415-420, 1996.

Sinton, J.M., D.S. Wilson, D.M. Christie, R.N. Hey, and J.R. Delaney, Petrologic consequences of rift propagation on oceanic spreading ridges, *Earth Planet. Sci. Lett.*, *62*, 193-201, 1983.

Small, C., Observations of ridge-hotspot interactions in the Southern Ocean, *J. Geophys. Res.*, *100*, 17,931-17,946, 1995.

Taylor, B., K. Crook, and J. Sinton, Extensional transform zones and oblique spreading centers, *J. Geophys. Res.*, *99*, 19,707-19,718, 1994.

Wessel, P., and W.H.F. Smith, Free software helps map and display data, *Eos Trans. AGU*, *72*, 441, 445-446, 1991.

Wilson D.S., Kinematics of overlapping rift propagation with cyclic rift failure, *Earth Planet. Sci. Lett.*, *96*, 384-392, 1990.

E. Bonatti, G. Bortoluzzi, G. Carrara, P. Fabretti, and M. Ligi, Istituto di Geologia Marina, Via P. Gobetti 101, 40129 Bologna, Italy. (bonatti@igm.bo.cnr.it; gb@igm.bo.cnr.cnr.it; carrara@igm.bo.cnr.it; fabretti@igm.bo.cnr.it; marcol@boigm2.igm.bo.cnr.it)

D. Gilod, Department of Geophysics, Moscow State University, Vorobievy Gory, Moscow 119899, Russia.

A. A. Peyve, S. Skolotnev, and N. Turko, Geological Institute of Russian Academy of Sciences, Pyzhevskiy pereulok 7, 109017 Moscow, Russia. (root@ginran.msk.su)

(Received September 23, 1998; revised April 22, 1999; accepted June 1, 1999.)